

AdvPC: Transferable Adversarial Perturbations on 3D Point Clouds

Abdullah Hamdi, Sara Rojas, Ali Thabet, Bernard Ghanem

King Abdullah University of Science and Technology (KAUST), Thuwal, Saudi Arabia

{abdullah.hamdi, sara.rojasmartinez, ali.thabet, Bernard.Ghanem} @kaust.edu.sa

Abstract

Deep neural networks are vulnerable to adversarial attacks, in which imperceptible perturbations to their input lead to erroneous network predictions. This phenomenon has been extensively studied in the image domain, and only recently extended to 3D point clouds. In this work, we present novel data-driven adversarial attacks against 3D point cloud networks. We aim to address the following problems in current 3D point cloud adversarial attacks: they do not transfer well between different networks, and they are easy to defend against simple statistical methods. To this extent, we develop new point cloud attacks (we dub AdvPC) that exploit input data distributions. These attacks lead to perturbations that are resilient against current defenses while remaining highly transferable compared to state-of-the-art attacks. We test our attacks using four popular point cloud networks: PointNet, PointNet++ (MSG and SSG), and DGCNN. Our proposed attack enables an increase in the transferability of up to 20 points for some networks. It also increases the ability to break defenses of up to 23 points on ModelNet40 data.

1. Introduction

Deep learning has shown impressive results in many perception tasks. Despite its performance, several works show deep learning algorithms susceptible to adversarial attacks. These attacks craft small perturbations to the inputs that push the network to produce incorrect outputs. There is significant progress made in 2D image adversarial attacks, where extensive work shows diverse ways to attack 2D based neural networks [27, 6, 12, 19, 3, 2, 37, 7]. In contrast, there is little focus on their 3D counterparts [32, 40, 39]. 3D point clouds, obtained with sensors like LiDAR, are now widely used in deep networks for safety-critical applications like self-driving cars [34, 11, 22]. However, as we will see in this paper, 3D deep networks are vulnerable to perturbations to their input, which increases the risk of using these models. In this paper, we present a novel approach to attack deep learning algorithms applied to 3D

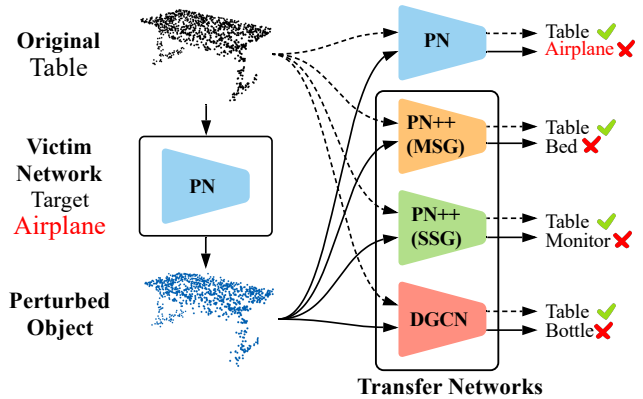


Figure 1: **Transferable Adversarial Perturbations on 3D point clouds:** Generating targeted attacks to fool PointNet [23](PN) by perturbing a Table point cloud. Not only does the perturbed 3D object force PointNet to predict the incorrect target class, but it also induces misclassification on the other networks (PointNet++ [24], DGCNN [30]) that are not involved in generating the perturbation.

point clouds and focus primarily on attack transferability between networks.

The concept of transferability has been extensively studied in the 2D image space [18, 20, 21]. Transferability allows an adversary to fool any network, without access to the network’s architecture. Clearly, transferable attacks pose a serious security concerns when deploying deep learning models. In this work, the goal is to generate adversarial attacks with network-transferability, *i.e.* the attack for a given input is generated using a single, accessible *victim* network and the perturbed sample to apply it on an unseen and inaccessible *transfer* network. Accessibility here refers to the parameters and architecture of the network. Figure 1 illustrates the concept of transferability. The perturbation generated by our method on a 3D object not only flips the class label of a victim network to the target class (*i.e.* it is adversarial), but it also induces a misclassification for the transfer networks that are not involved in generating the perturbation (*i.e.* it is transferable).

Very few adversarial attacks have been developed for 3D

point clouds since the first method introduced by Xiang *et al.* [32], which proposes two attack modes, point perturbation, and adversarial point generation. We identify two chief shortcomings in current 3D adversarial attack methods [32, 40]. First, their attacks are unsuccessful in the presence of simple defenses, such as Statistical Outlier Removal [40]. Second, they are limited to the victim network and do not transfer to other networks [32]. In contrast, our work not only focuses on adversarial perturbations that are significantly more resilient against currently available point cloud defenses but also on those that transfer well between different point cloud networks. Inspired by [20] and to generate more transferable attacks, we use a point cloud Auto-Encoder (AE), which can effectively reconstruct the original input from the perturbation, and then add a data adversarial loss. We optimize the perturbation added to the sample perturbed sample to fool the classifier *before* (regular adversarial loss) and *after* it passes through the AE (data adversarial loss). In doing so, the attack tends to be less dependant on the victim network, and generalizes better to different networks. We dub this attack *AdvPC*, and our full pipeline is optimized end-to-end from the classifier output to the perturbation.

Contributions: Our contributions are two-fold. (1) We propose a new pipeline and loss function, to perform transferable adversarial perturbations on 3D point clouds. Our approach trade-off success of attacking the victim network with transferability to the transfer networks by introducing a data adversarial loss targeting the victim network after reconstructing with a point cloud AE. (2) We perform extensive experiments under constrained norm-budgets to validate the transferability of our attacks. We transfer our attacks between four point cloud networks and show superiority against the state-of-the-art under the same norm-budgets. Furthermore, we demonstrate how our attacks outperform others against all available point cloud defenses.

To the best of our knowledge, we are the first to introduce network-transferable adversarial perturbations on 3D point clouds. Our attacks are optimized on one accessible victim network and can be used to attack other networks that are inaccessible directly.

2. Related Work

2.1. Deep Learning for 3D Point Clouds

PointNet [23] paved the way as the first deep learning algorithm to operate directly on 3D point clouds. PointNet computes point features independently, and aggregates them using an order invariant function like max-pooling. An update to this work was PointNet++ [24], where points are aggregated at different 3D scales. Subsequent work focused on how to aggregate more local context [4] or on more complex aggregation strategies like RNNs [8, 35]. More re-

cent methods run convolutions across neighbors of points, instead of using point-wise operations [30, 16, 28, 14, 13, 16, 29, 15]. Contrary to PointNet and its variants, these works achieve superior recognition results by focusing on local feature processing. In this paper to evaluate and validate our adversarial attacks, we use three point-wise networks, PointNet [23] and PointNet++ [24] in single-scale (SSG) and multi-scale (MSG) form, and a point convolution network, DGCNN [30]. We show the transferability of AdvPC attacks between these four networks and we study the sensitivity of each network to adversarial perturbations.

2.2. Adversarial Attacks

Pixel-based Adversarial Attacks. Initial work on image-based adversarial attacks was introduced by Szegedy *et al.* [27], who cast the attack problem as optimization with pixel perturbations being minimized, to fool a trained classifier to predict a wrong class label. Since then, the topic of adversarial attacks has attracted much attention [6, 12, 19, 3, 17]. More recent works take a learning-based approach to the attack [20, 21, 38]. They train a neural network (adversary) to perform the attack on the training data and then use the trained adversary model to attack unseen samples. The work of Zhao *et al.* [38] uses a trained GAN [5] to generate natural images and optimizes the latent vector to generate natural adversarial examples. On the other hand, the work by Nasser *et al.* [20] uses an AE to learn transferable adversarial pixel perturbations. This work closely relates to our formulation, and we adapt its main concepts to fit the irregular nature of 3D point clouds. Our work differs from theirs in that we tackle network-transferability while they focus on learning to attack domains that are not accessible by the adversary (domain-transferability).

Adversarial Attacks Beyond Images. Several adversarial attacks have moved beyond pixel perturbations. One line of work focuses on attacking object pose [7, 37, 2], while other methods investigate perturbations on object shape [33]. However, all of these attacks target 2D CNNs that operate on the image space. Recently, Xiang *et al.* [32] developed adversarial perturbations on 3D point clouds. Their proposed method successfully generates attacks on PointNet [23]; however, they have two main shortcomings. First, they can be easily defended by simple statistical operations [40]. Second, the attacks are non-transferable and only work on the attacked network [32, 40]. In contrast, Zheng *et al.* [39] proposed dropping points from the point cloud using a saliency map, to fool trained 3D deep networks. As compared to [32], our proposed attacks are significantly more successful against available defenses and more transferable beyond the attacking network. As compared to [39], our attacks are modeled as an optimization on the perturbation variable directly with a focus on point perturbations instead of point removal.

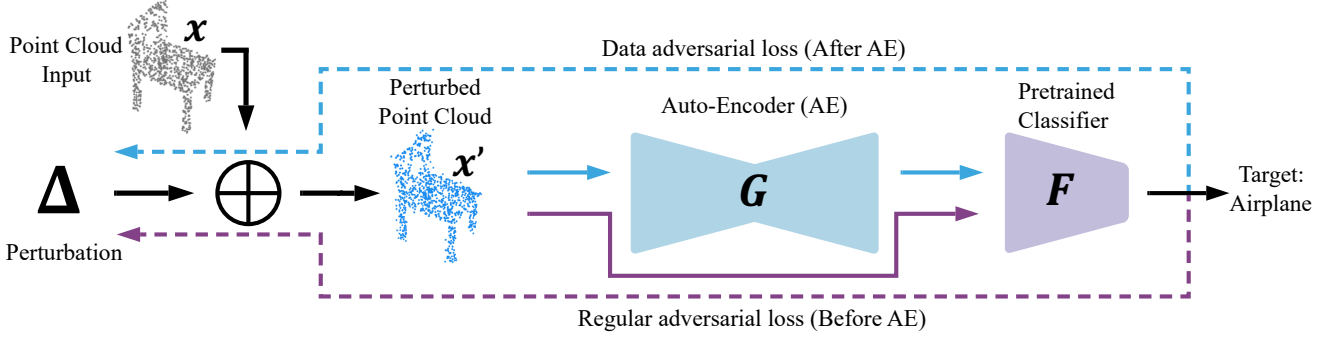


Figure 2: **AdvPC Attack Pipeline:** We optimize for the constrained perturbation variable Δ , such that the perturbed sample $\mathcal{X}' = \mathcal{X} + \Delta$ fools a trained classifier \mathbf{F} (i.e. $\mathbf{F}(\mathcal{X}')$ is incorrect), and the same classifier if the attack is reconstructed by an Auto-Encoder (AE) \mathbf{G} (i.e. $\mathbf{F}(\mathbf{G}(\mathcal{X}'))$ is incorrect). The adversarial loss on network \mathbf{F} is defined as in Eq (3) and has two parts controlled by hyperparameter γ : network adversarial loss (*top*) and data adversarial loss (*bottom*). Dotted lines are gradients flowing to the perturbation variable Δ .

Defending Against 3D Point Cloud Attacks. Zhou *et al.* [40] proposed a Statistical Outlier Removal (SOR) method as a defense against point cloud attacks. SOR uses k-Nearest Neighbors (kNN) to identify and remove point outliers. The logic here is that these outliers usually correspond to “unnatural” points created by the attack. As such, they proposed DUP-Net, which is a combination of their SOR and a point cloud up-sampling network PU-Net [36]. Zhou *et al.* also proposed removing unnatural points by Simple Random Sampling (SRS), where each point has the same probability of being removed. In this paper, we present and thoroughly analyze new attacks that prove to be stronger against the mentioned defenses.

3. Methodology

The pipeline of AdvPC is depicted in Figure 2. It consists of an Auto-Encoder (AE) denoted by \mathbf{G} , which is trained to reconstruct 3D point cloud data, and a point cloud classifier denoted by \mathbf{F} . We seek to find a perturbation variable Δ that fools \mathbf{F} before *and* after it passes through the AE for reconstruction. The setup makes the attack less dependant on the victim network and more dependent on the data (represented by the AE). As such, we expect this strategy to generalize to different networks. In this section, we first describe the main components of our pipeline: 3D point cloud input, AE, and point cloud classifier. We then present our attack setup and loss.

3.1. Attack Pipeline

3D Point Clouds (\mathcal{X}). We define a point cloud $\mathcal{X} \in \mathbb{R}^{N \times 3}$, as a set of N 3D points, where each point $\mathbf{x}_i \in \mathbb{R}^3$ is represented by its 3D coordinates (x_i, y_i, z_i) .

Point Cloud Networks (\mathbf{F}). We focus on 3D point cloud classifiers with a feature max pooling layer as detailed in Eq (1), where h_{conv1D} and h_{mlp} are a 1D convolution and an

MLP, respectively, to produce the K -class classifier \mathbf{F} .

$$\mathbf{F}(\mathcal{X}) = h_{\text{mlp}}\left(\max_{\mathbf{x}_i \in \mathcal{X}} \{h_{\text{conv1D}}(\mathbf{x}_i)\}\right) \quad (1)$$

Here $\mathbf{F} : \mathbb{R}^{N \times 3} \rightarrow K$ produces the logits layer of the classifier with size K . For our attacks, we take \mathbf{F} to be one of the following widely used networks in the literature: PointNet [23], PointNet++ [24] in single-scale form (SSG) and multi-scale form (MSG), and DGCNN [30]. Each network manifests different behaviors under random perturbations. Section 5.2 delves deep into these differences and their effect on the transferability of the attacks and robustness of each network to perturbations.

Point Cloud Auto-Encoder (\mathbf{G}). An AE learns a representation of the data and acts as an effective defense against adversarial attacks. It ideally projects a perturbed point cloud onto the natural manifold of inputs. Any AE architecture in point clouds can be used in our pipeline, but we select the one in [1] given its simple structure and effectiveness in recovering from adversarial perturbation. The AE \mathbf{G} consists of an encoding part, $\mathbf{g}_{\text{encode}} : \mathbb{R}^{N \times 3} \rightarrow \mathbb{R}^q$, which produces a latent vector $\mathbf{z} \in \mathbb{R}^q$ that can in turn be decoded using an MLP, $\mathbf{g}_{\text{mlp}} : \mathbb{R}^q \rightarrow \mathbb{R}^{N \times 3}$, to produce a point cloud. It can be described formally as: $\mathbf{G}(\mathcal{X}) = \mathbf{g}_{\text{mlp}}(\mathbf{z})$ with $\mathbf{z} = \mathbf{g}_{\text{encode}}(\mathcal{X})$. Here, $\mathbf{g}_{\text{encode}}$ is defined as in Eq (1). We train the AE with the Chamfer loss as in [1] on the same data used to train \mathbf{F} , such that it can reliably encode/decode 3D point clouds. The AE is then kept fixed during the optimization of the adversarial perturbation. We show in Section 4.2 how the AE acts as an effective defense against point cloud adversarial perturbations. The AE learns how naturally occurring point clouds look like. Therefore, This composition allows the crafted attack to successfully attack the victim classifier, as well as fool other classifiers that are not seen by the attacker but operate on a similar data manifold. Furthermore, since many of the available points, cloud defenses

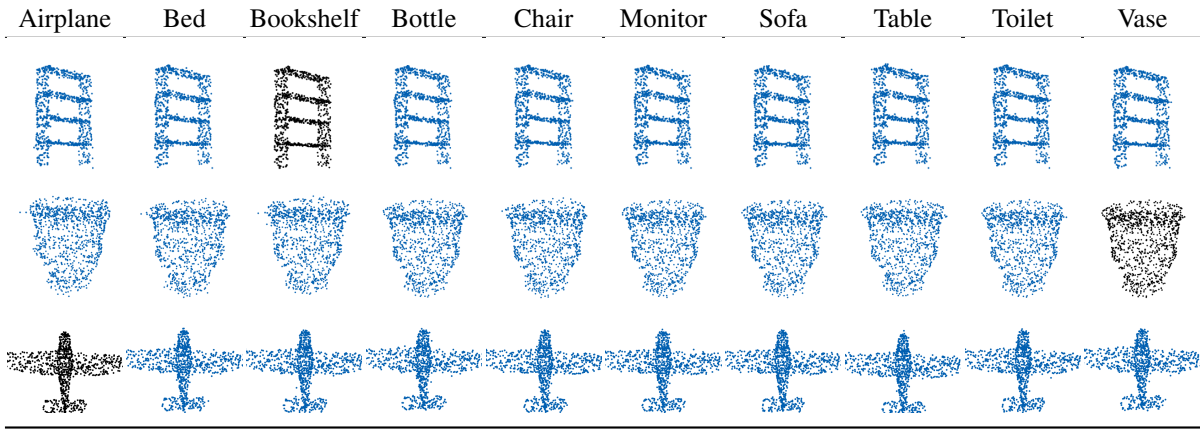


Figure 3: **Examples of AdvPC Attacks:** Adversarial perturbations performed on victim networks PointNet (*top*), PointNet ++ MSG (*middle*), and PointNet ++ SSG (*bottom*). The original objects are in black under their true class label, while the perturbed examples are in blue under their false target label of the successful attack.

rely on natural statistics of 3D point clouds [40], succeeding to attack the classifier after AE reconstruction also leads to perturbations resilient to those defenses.

3.2. 3D Adversarial Perturbations

Proposed Attack. In AdvPC attacks, like the ones in Figure 3, we focus solely on perturbations of the input. This means we modify each point \mathbf{x}_i by a perturbation variable. Formally, we define the perturbed point set $\mathcal{X}' = \mathcal{X} + \Delta$, where $\Delta \in \mathbb{R}^{N \times 3}$ is the perturbation parameter we are optimizing for. Consequently, each pair $(\mathbf{x}_i, \mathbf{x}'_i)$ are in correspondence. Adversarial attacks are commonly formulated as in Eq (2), where the goal is to find an input perturbation Δ that successfully fools \mathbf{F} to predict an incorrect target label t' , while keeping \mathcal{X}' and \mathcal{X} close using distance metric $\mathcal{D}: \mathbb{R}^{N \times 3} \times \mathbb{R}^{N \times 3} \rightarrow \mathbb{R}$. The formulation in Eq (2) is usually known as a targeted attack.

$$\min_{\Delta} \mathcal{D}(\mathcal{X}, \mathcal{X}') \quad \text{s.t.} \quad \left[\max_i \mathbf{F}(\mathcal{X}'_i) \right] = t' \quad (2)$$

As pointed out in [3], it is difficult to directly solve Eq (2). Instead, previous works like [32] have used the well-known C&W formulation, giving rise to the commonly known soft constraint attack: $\min_{\Delta} f_{t'}(\mathbf{F}(\mathcal{X}')) + \lambda \mathcal{D}(\mathcal{X}, \mathcal{X}')$ where $f_{t'}(\mathbf{F}(\mathcal{X}'))$ is the targeted adversarial loss function defined on the network \mathbf{F} to move it to target t' as in Eq (3).

$$f_{t'}(\mathbf{F}(\mathcal{X}')) = \left(\max_{i \neq t'} (\mathbf{F}(\mathcal{X}'_i) - \mathbf{F}(\mathcal{X}'_{t'})) \right)^+ \quad (3)$$

Alternatively, we can formulate Eq (2) using hard constraints as in Eq (4), where the objective can be minimized using Projected Gradient Descent (PGD) similar to what is done in the image domain [12, 17].

$$\min_{\Delta} f_{t'}(\mathbf{F}(\mathcal{X}')) \quad \text{s.t.} \quad \mathcal{D}(\mathcal{X}, \mathcal{X}') \leq \epsilon \quad (4)$$

Using a hard constraint sets a limit to the amount of added perturbation in the attack. This limit is defined by ϵ in Eq (4). Having this bound ensures fair comparisons between different attacks schemes. We can do these comparisons by measuring the effectiveness of these attacks at different levels of ϵ . Using PGD, the above optimization in Eq (4) with L_p distance $\mathcal{D}_{L_p}(\mathcal{X}, \mathcal{X}')$ can be solved by iteratively projecting the perturbed sample onto the L_p sphere of size ϵ_p such that: $\Delta_{t+1} = \Pi_p(\Delta_t - \eta \nabla_{\Delta_t} f_{t'}(\mathbf{F}(\mathcal{X}')), \epsilon_p)$ Here, $\Pi_p(\Delta, \epsilon_p)$ projects the perturbation Δ onto the L_p sphere of size ϵ_p , and η is a step size. The two most commonly used L_p distance metrics in the literature are L_2 , which measures the energy of the perturbation, and L_∞ , which measures the maximum point perturbation of each $\delta_i \in \Delta$. Our experiments use the L_2 distance defined as $\mathcal{D}_{L_2}(\mathcal{X}, \mathcal{X}') = (\sum_i \|\delta_i\|_2^2)^{\frac{1}{2}} = \|\Delta\|_F$, while the projection of Δ onto the L_2 sphere of size ϵ_2 is: $\Pi_2(\Delta, \epsilon_2) = \frac{\epsilon_2}{\max(\|\Delta\|_F, \epsilon_2)} \Delta$. The norm-budget ϵ_2 is the one used throughout the experiments in this work.

In **Appendix**, we detail our formulation when L_∞ is used as the distance metric and report similar superiority over the baselines as the L_2 results in Section 4.2. For completeness, we also show in the supplement the effect of using different distance metrics (L_2 , Chamfer, and Earth Mover Distance) as soft constraints on limiting the transferability and effectiveness of the attacks as well as demonstrating the learning approach instead of optimization.

Data Adversarial Loss. The objectives in Eq (2, 4) focus solely on the network \mathbf{F} . We also want to add more focus on the data in crafting our attacks. We do so by fooling \mathbf{F}

Victim Network	Attack	Success Rate	$\epsilon_2 = 1.8$				$\epsilon_2 = 4$				
			PN	PN++ (MSG)	PN++ (SSG)	DGCNN	Success Rate	PN	PN++ (MSG)	PN++ (SSG)	DGCNN
-	No attack	-	92.8	91.5	91.5	93.7	-	92.8	91.5	91.5	93.7
-	Random	0	73.7	33.3	6.2	46.2	0	32.8	1.7	0.4	0.8
PN	Baseline [32]	100	-	89.7	90.5	93.1	100	-	89.6	90.1	93.1
	AdvPC (Ours)	99.9	-	89.0	86.8	91.0	99.9	-	89.2	88.6	92.5
PN++ (MSG)	Baseline [32]	100	92.4	-	88.1	93.0	100	91.1	-	86.2	92.0
	AdvPC (Ours)	99.2	90.3	-	82.8	91.2	99.2	84.8	-	76.8	83.8
PN++ (SSG)	Baseline [32]	100	92.8	91.7	-	94.4	100	92.8	91.4	-	94.3
	AdvPC (Ours)	100	92.2	91.4	-	94.1	100	92.0	91.1	-	94.4
DGCNN	Baseline [32]	99.6	89.4	88.4	83.0	-	99.7	81.9	87.8	68.8	-
	AdvPC (Ours)	98.3	76.5	77.6	64.6	-	98.3	69.2	70.8	60.0	-

Table 1: **Transferability of Attacks:** We use norm-budgets $\epsilon_2 = 1.8$ and $\epsilon_2 = 4$. All the reported results (other than the attack success rate) are classification accuracies on the attack set (**lower** numbers are better attacks). Our attack consistently achieves better transferability than the baseline for all networks, especially on DGCNN [30]. We also note that DGCNN is the hardest network to attack and generally transfers better than other networks. The original accuracy of the networks under no attack, random perturbations with the same ϵ_2 as the attacks, and the success rate of all attacks are all put for reference.

using both the perturbed input \mathcal{X}' and the AE reconstruction $\mathbf{G}(\mathcal{X}')$ (see Figure 2). Our new objective becomes:

$$\min_{\Delta} \mathcal{D}(\mathcal{X}, \mathcal{X}') \quad (5)$$

$$\text{s.t. } [\max_i \mathbf{F}(\mathcal{X}')_i] = t'; [\max_i \mathbf{F}(\mathbf{G}(\mathcal{X}'))_i] \neq [\max_i \mathbf{F}(\mathcal{X}')_i]$$

The first constraint is the same as the one in Eq (2), while the second constraint ensures that the prediction of the perturbed sample after the AE differs from the true label of the clean sample. However, just like Eq (2), this objective is hard to optimize, so we follow similar steps as in Eq (4) and optimize for the following main objective of AdvPC using PGD (assuming using L_2 as the distance metric):

$$\min_{\Delta} (1 - \gamma) f_{t'}(\mathbf{F}(\mathcal{X}')) + \gamma f_{t''}(\mathbf{F}(\mathbf{G}(\mathcal{X}')))$$

$$\text{s.t. } \mathcal{D}_{L_2}(\mathcal{X}, \mathcal{X}') \leq \epsilon_2 \quad (6)$$

Here, t'' is any false label $t'' \neq \max_i \mathbf{F}(\mathcal{X}')_i$ and γ is the hyper-parameter that trades off the attack successes before and after the AE. The baseline attack we use in our experiments is a special case of Eq (6), when $\gamma = 0$. This is the same attack as in Eq (4) and very similar to [32], if put under constraint. We use PGD to solve Eq (6) just like Eq (4). We follow the same procedure as in [32] when solving the optimization in Eq (6) by keeping a record of any Δ that satisfies the constraints in Eq (5) and by trying different initializations for Δ .

4. Experiments

4.1. Setup

Dataset and Networks. We use ModelNet40 [31] to train the classifier network (\mathbf{F}) and the AE network (\mathbf{G}), as well as test our attacks. ModelNet40 contains 12,311 CAD models from 40 different classes. CAD models are divided into

9,843 for training and 2,468 for testing. Similar to previous work [40, 32, 39], we sample 1,204 points from each object. We train the \mathbf{F} victim networks: PointNet[23], PointNet++ in both Single-Scale (SSG) and Multi-scale (MSG) [24] settings, and DGCNN [30]. The four networks were trained for 250 epochs. For a fair comparison, we adopt the subset of ModelNet40 detailed in [32] to perform and evaluate our attacks against their work (we call attack set). In this subset, 250 examples are chosen from 10 ModelNet40 classes. Following the setup in [32], we create pairs of victim networks and target labels in the attacks to generate 2,250 attacks per ϵ_2 . The accuracies of trained networks on the attack set before adding perturbations are shown in Table 1. We train the AE using the full ModelNet40 training set with the Chamfer Distance loss for 500 epochs and then fix the AE when the attacks are being generated. Here we note that r-GAN and l-GAN from [1] were investigated instead of the AE, but the latter lead to worse performance. Refer to the **Appendix** for more details and further experiments.

Transferability. We follow the same setup as [20, 21] by generating attacks using the constrained L_2 metric and measure their success rate at different norm-budgets ϵ_2 . We compare AdvPC ($\gamma = 0.5$) against the baseline [32] without the data adversarial loss ($\gamma = 0$). the use of $\gamma = 0.5$ specifically for AdvPC is motivated by striking a balance between the success of the attack and its transferability (refer to Section 5.1 for details). To measure the success of the attack, we measure the percentage of samples out of all attacked samples that the victim network classified as the target. We also measure transferability from each victim network to the transfer networks. For each pair of networks, we optimize the attack on one network and test the classification accuracy on the transfer networks. We report these numbers for all network pairs. The range of norm-budget ϵ_2 in our experiments is taken to be [0, 7]. We use Adam optimizer

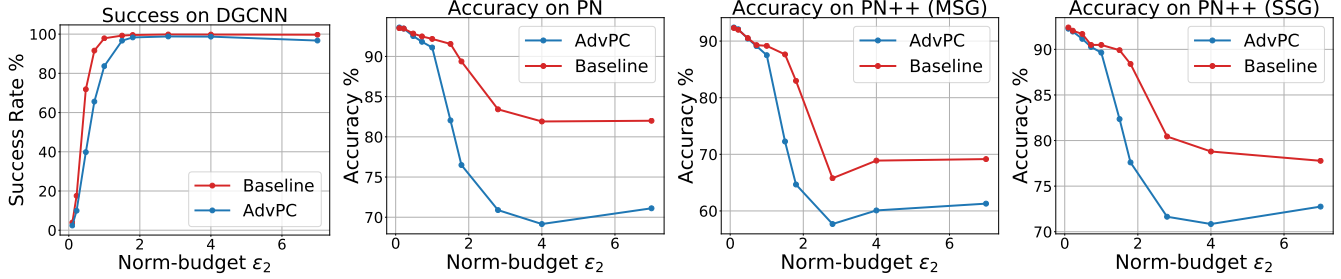


Figure 4: **Transferability Across Different Norms:** Attack performed using DGCNN [30] across different ϵ_2 norm-budgets. We report the success on the victim network and the accuracy on the transfer networks (PointNet, PointNet ++ MSG, PointNet++ SSG). We note that AdvPC transfers better to other networks with bigger ϵ_2 compared to the baseline [32].

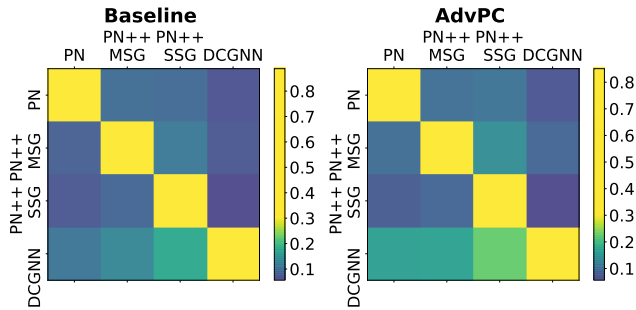


Figure 5: **Transferability Matrix:** Visualizing all the transferability across all the norm-budgets ϵ_2 for AdvPC (right) and Baseline [32] (left). Every row is the victim network used in the attack, and every column is the transfer network transferability score of that attack. Brighter colors in the diagonal indicate self-transferability, while AdvPC transferability matrix is generally brighter than the baseline [32], indicating better transferability. Also, we notice that the DGCNN attacks tend to be brighter off-diagonal than the other rows, indicating more transferability than other networks. The transferability score is 1 minus the average transfer accuracy across all the ϵ_2 as detailed in Section 4.2.

[10] with learning rate $\eta = 0.01$, and perform 4 different initializations for the optimization of Δ . The number of iterations for the attack optimization for PN, PN++ MSG, PN++ SSG, and DGCNN are 500, 500, 500, and 700, respectively (DGCNN requires more iterations).

Attacking the Defenses. We also analyze the success of our attacks against point cloud defenses. We compare AdvPC attacks and the baseline [32] against several defenses used in the point cloud literature: SOR, SRS, DUP-Net [40], Adversarial Training [32], and the AE we trained. For SRS, we use a drop rate of 10%, while in SOR, we use the same values proposed in [40]. We train DUP-Net on ModelNet40 with an up-sampling rate of 2. For Adversarial Training, all 4 networks are trained using a mix of the training data of ModelNet40 and adversarial attacks generated by [32].

Defenses	$\epsilon_2 = 1.5$		$\epsilon_2 = 1.8$	
	Baseline [32] ($\gamma = 0$)	AdvPC ($\gamma = 0.5$)	Baseline [32] ($\gamma = 0$)	AdvPC ($\gamma = 0.5$)
No defense	0.8	3.3	0.4	1.7
AE	89.5	3.5	88.5	1.7
Adv Training [32]	99.1	97.1	99.0	96.3
SOR [40]	85.7	83.6	84.5	82.0
DUP Net [40]	88.4	87.28	88.0	86.13
SRS [40]	83.2	61.6	75.4	53.2

Table 2: **Attacking Point Cloud Defenses:** We evaluate our attack using norm-budgets of $\epsilon_2 = 1.5$ and $\epsilon_2 = 1.8$ using DGCNN [30] on different defenses of 3D point clouds. The reported numbers are accuracies on the attack set (**lower** indicates better attack). The accuracy of DGCNN on the clean attack set is 93.7 %.

4.2. Results

We first highlight some qualitative results in Figure 3 that show evidence of naturally looking perturbed examples, which can fool point cloud networks. Below, we present quantitative results focused on two main aspects. First, we show the transferable power of our attacks between different point cloud networks. Second, we highlight the strength of our pipeline under different point cloud defenses.

Transferability. Table 1 shows transferability results for $\epsilon_2 = 1.8$ and $\epsilon_2 = 4$ and compares AdvPC ($\gamma = 0.5$) with the baseline [32] ($\gamma = 0.5$). AdvPC attacks consistently beat the baseline when transferring between networks. Our method shows substantial gains when optimized for DGCNN. We also report transferability results for a range of ϵ_2 values in Figure 4, which shows results for victim network DGCNN transferred to all other networks. Instead of plotting these curves for all transferability experiments, we aggregate their results using a Transferability Matrix (refer to Figure 5 for an example). Every entry in this matrix scores the transferability from the victim network (rows) to the transfer network (columns), and it is computed as 1 minus the average accuracy of the transfer network across all ϵ_2 values. This number reflects how good the perturbation is at fooling the transfer network overall.

γ	0	0.25	0.5	0.75	0.9	1
Success Rate	99.5	98.8	97.6	97.3	94.5	4.0
Transferability	13.1	20.0	27.2	29.0	32.1	8.5

Table 3: Ablation Study: Studying the effect of changing the hyperparameter in our attack (γ) on the success rate of the attack and on its transferability (1- average accuracy of transfer networks). The network used in the attack is DGCNN [30], and the attack is performed with $\epsilon_2 = 1.8$. We note that as γ increases, the success rate of the attack drops while the transferability increases, which highlights the trade-off between success and transferability observed throughout our work.

We show the transferability matrix for our attack ($\gamma = 0.5$) and the baseline ($\gamma = 0$) in Figure 5. AdvPC transfers better overall since it induces higher (brighter) off-diagonal values in the matrix. If we average the off-diagonal elements of this matrix, we get an 11.2% mean transferability score for AdvPC, as compared to 9.4% for the baseline ($\gamma = 0$). If we average the success rates of all the victim networks for AdvPC and on all the norm-budgets ϵ_2 , we get 76.3%, as compared to 81.5% for the baseline. We note that DGCNN [30] performs best in terms of transferability and is the hardest network to attack (on both AdvPC and baseline). This observation is similar to [18] in 2D image domain with regards to VGG-19 [26] transferability. These results highlight the inherent trade-off between attack success and transferability. We further explore this trade-off in Section 5.1.

Attacking Defenses. Since DGCNN performs the best in transferability, we use it to evaluate the resilience of our attacks under different defenses. We use the 5 defenses described in Section 4.1 and report their results in Table 2. Note that the trained AE we use in AdvPC is an effective defense against the previous attacks [32] as it recovers the original accuracy (89%). Our attack is more resilient than the baseline against all defenses. Our attack is strongest against the AE defense (85% improvement against the baseline), which we expect since we use the AE in our optimization. We also see our attack is strong against simple statistical point removal like SRS (30% improvement against the baseline). We show similar quantitative results for other setups in the **Appendix**.

5. Analysis

We perform several analytical experiments to explore further the results obtained in Section 4.2. We first study the effect of different factors that play a role in the transferability of our attacks. We also show some interesting insights related to the interpretability of point cloud networks. For a more comprehensive analysis and visualizations of our methods and results, please refer to the **Appendix**.

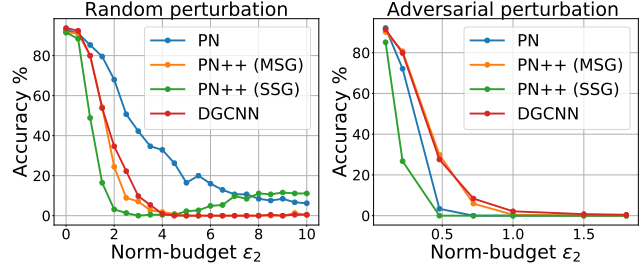


Figure 6: Sensitivity of Architectures: we evaluate the accuracy of different networks under constrained norm random perturbation (left) and adversarial perturbation (right) with $\gamma = 0.5$. We note that PointNet [23] is the most robust under random perturbations, while DGCNN [30] is the most robust to adversarial perturbations.

5.1. Ablation Study (hyperparameter γ)

Here, we study the effect of the hyperparameter γ used in Eq (6) on the performance of our attacks. We fix the victim network to be DGCNN [30] and limit the norm-budget $\epsilon_2 = 1.8$. Then, we vary γ between 0 (the baseline [32]) and 1 and record the success rate and transferability of the attack to the other three networks (as measured in Section 4.2). We present our results in Table 3. One observation is that, while adding the AE loss with $\gamma > 0$ indeed improves transferability, it causes the success to deteriorate. We pick $\gamma = 0.5$ in our experiments to balance success and transferability.

5.2. Sensitivity of Networks

Figure 6 shows the sensitivity of the various networks, when they are submitted to input perturbations of varying norm-budgets ϵ_2 . We evaluate the accuracy of different networks under random perturbation and adversarial perturbations with $\gamma = 0.5$. We note that PointNet [23] is the most robust under random perturbations due to its global max-pooling layer that neglects neighborhood information of each point in the point cloud. On the other hand, DGCNN [30] tends to be the most robust to adversarial perturbations. In DGCNN, convolution neighborhoods are dynamically updated across layers and epochs. This dynamic behavior adds extra randomness, which hinders the job of the attack, leading to lower success. The relation between randomness and robustness is also established in [25].

5.3. Accuracy vs. Robustness

Here, we want to study the relationship between the accuracy of a 3D deep network and its robustness, as it has been investigated extensively in the image domain. To remove the bias of initial network accuracy (*i.e.* no perturbation) in our results, we normalize the accuracy vs. ϵ_2 plot by the initial accuracy (*i.e.* when $\epsilon_2 = 0$). We focus on DGCNN [30] as the network to be analyzed and train it for different epochs (1, 11, and 250) to obtain different networks

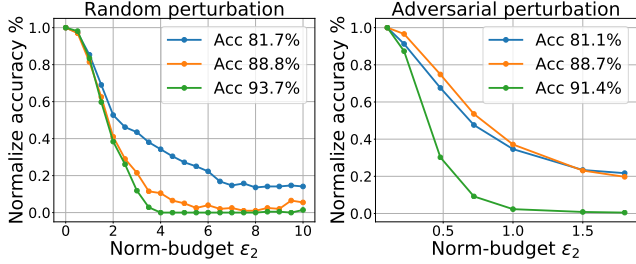


Figure 7: **Accuracy vs Robustness:** The normalized accuracy of different DGCNN [30] trained with different accuracies and evaluated under random perturbations (*left*) and adversarial perturbation with $\gamma = 0.5$ (*right*).

with identical architectures but with different initial accuracies (81.7 %, 88.8 %, and 93.7 %). We plot the normalized accuracy under random perturbation and under adversarial perturbation ($\gamma = 0.5$) with different ϵ_2 for all these networks in Figure 7. We observe how less accurate networks are more robust to losing initial accuracy if subjected to both random or adversarial perturbation. This observation of inverse relation between accuracy and robustness is well-known in the image domain [9].

5.4. Natural-looking Attacks

We show qualitative comparisons between AdvPC ($\gamma = 0.5$) and the baseline [32] ($\gamma = 0$) in Figure 8. We use PointNet as the victim, and we see how the baseline [32] produces visible outlier points in the attack (highlighted by the green circles), while AdvPC does not suffer from this problem. We argue that these artifacts are not natural, and by removing them, we destroy the attack and recover the original accuracy. This observation aligns with the results of the outlier removal defense (SOR) on the baseline attack in Table 2. We also argue that using the data adversarial loss with $\gamma > 0$ gives attack some knowledge of the natural data manifold, thus reducing the effect observed in Figure 8.

5.5. Interpretability

One advantage of adding the AE to the attack pipeline is that it reveals some semantic relations between the different object classes. Since we are not enforcing a specific false target t'' for the data adversarial loss on the reconstructed point cloud in Eq (6), t'' is picked dynamically by the optimization to be a *similar* class to the original class. For example, a perturbed Bottle by AdvPC would transform into a Vase if reconstructed by the AE. The Bottle class and the Vase class look *similar*. We see this effect in Figure 9, where we visualize the perturbed point clouds before and after the AE reconstruction. For example, we observe that our attacks on a *bottle* force the AE to reconstruct a *vase*. This effect is not observed in the other attacks, and it il-

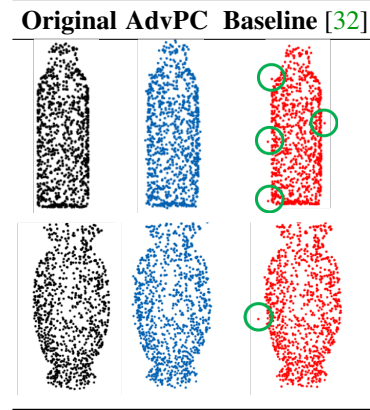


Figure 8: **Qualitative Comparison:** Comparing AdvPC to the baseline [32]. We observe that AdvPC does not suffer from the outlier points (highlighted in the baseline) which makes the attack easily defended by simple statistics as done in [40].

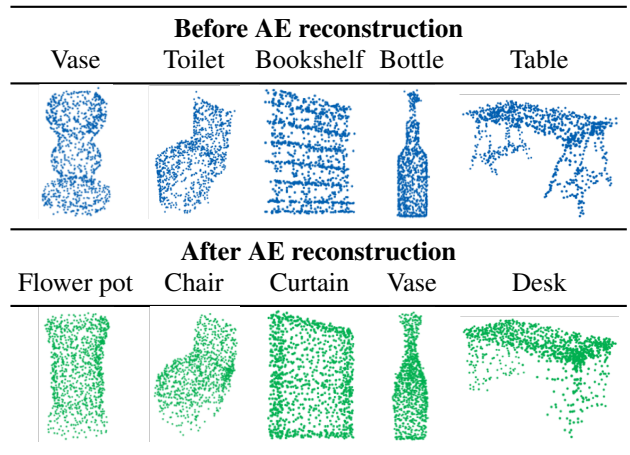


Figure 9: **Interpretability of AdvPC:** Attacked samples before reconstruction (*top*) and after reconstruction (*bottom*) by the AE. Perturbed samples by AdvPC, if passed through the AE, transform into similar objects but from different classes. This illustrates some information about what the representation learned by the victim network and the AE.

lustrates some information about the representation of the objects learned by the victim network as well as the AE.

6. Conclusions

In this paper, we propose a new attack for 3D point clouds that utilizes a data adversarial loss to formulate network-transferable perturbations. Our attacks show better transferability between 4 popular point cloud networks as well as improve state-of-the-art against defenses. Future direction would include other 3D deep learning tasks, such as detection and segmentation. Another line of work that naturally extends our work is to develop robust models.

References

- [1] Panos Achlioptas, Olga Diamanti, Ioannis Mitliagkas, and Leonidas Guibas. Learning representations and generative models for 3d point clouds. *arXiv preprint arXiv:1707.02392*, 2017. [3](#), [5](#), [12](#), [28](#), [29](#)
- [2] Michael A. Alcorn, Qi Li, Zhitao Gong, Chengfei Wang, Long Mai, Wei-Shinn Ku, and Anh Nguyen. Strike (with) a pose: Neural networks are easily fooled by strange poses of familiar objects. In *The IEEE Conference on Computer Vision and Pattern Recognition (CVPR)*, June 2019. [1](#), [2](#)
- [3] Nicholas Carlini and David Wagner. Towards evaluating the robustness of neural networks. In *IEEE Symposium on Security and Privacy (SP)*, 2017. [1](#), [2](#), [4](#), [12](#)
- [4] Francis Engelmann, Theodora Kontogianni, Alexander Hermans, and Bastian Leibe. Exploring spatial context for 3d semantic segmentation of point clouds. feb 2018. [2](#)
- [5] Ian Goodfellow, Jean Pouget-Abadie, Mehdi Mirza, Bing Xu, David Warde-Farley, Sherjil Ozair, Aaron Courville, and Yoshua Bengio. Generative adversarial nets. In Z. Ghahramani, M. Welling, C. Cortes, N. D. Lawrence, and K. Q. Weinberger, editors, *Advances in Neural Information Processing Systems 27*, pages 2672–2680. Curran Associates, Inc., 2014. [2](#)
- [6] Ian Goodfellow, Jonathon Shlens, and Christian Szegedy. Explaining and harnessing adversarial examples. In *International Conference on Learning Representations*, 2015. [1](#), [2](#), [13](#)
- [7] Abdullah Hamdi, Matthias Müller, and Bernard Ghanem. SADA: semantic adversarial diagnostic attacks for autonomous applications. *CoRR*, abs/1812.02132, 2018. [1](#), [2](#)
- [8] Qiangui Huang, Weiyue Wang, and Ulrich Neumann. Recurrent slice networks for 3d segmentation of point clouds. In *Proceedings of the IEEE Conference on Computer Vision and Pattern Recognition*, pages 2626–2635, 2018. [2](#)
- [9] Andrew Ilyas, Shibani Santurkar, Dimitris Tsipras, Logan Engstrom, Brandon Tran, and Aleksander Madry. Adversarial examples are not bugs, they are features. In *ArXiv preprint arXiv:1905.02175*, 2019. [8](#)
- [10] Diederik P. Kingma and Jimmy Ba. Adam: A method for stochastic optimization. *CoRR*, abs/1412.6980, 2014. [6](#)
- [11] Jason Ku, Melissa Mozifian, Jungwook Lee, Ali Harakeh, and Steven L Waslander. Joint 3d proposal generation and object detection from view aggregation. In *2018 IEEE/RSJ International Conference on Intelligent Robots and Systems (IROS)*, pages 1–8. IEEE, 2018. [1](#)
- [12] Alexey Kurakin, Ian J. Goodfellow, and Samy Bengio. Adversarial machine learning at scale. *CoRR*, abs/1611.01236, 2016. [1](#), [2](#), [4](#), [12](#), [13](#)
- [13] Loic Landrieu and Mohamed Boussaha. Point cloud oversegmentation with graph-structured deep metric learning. pages 7440–7449, 2019. [2](#)
- [14] Loic Landrieu and Martin Simonovsky. Large-scale point cloud semantic segmentation with superpoint graphs. In *Proceedings of the IEEE Conference on Computer Vision and Pattern Recognition*, pages 4558–4567, 2018. [2](#)
- [15] Jiaxin Li, Ben M Chen, and Gim Hee Lee. So-net: Self-organizing network for point cloud analysis. In *Proceedings of the IEEE conference on computer vision and pattern recognition*, pages 9397–9406, 2018. [2](#)
- [16] Yangyan Li, Rui Bu, Mingchao Sun, Wei Wu, Xinhan Di, and Baoquan Chen. Pointcnn: Convolution on x-transformed points. In *Advances in Neural Information Processing Systems*, pages 820–830, 2018. [2](#)
- [17] Aleksander Madry, Aleksandar Makelov, Ludwig Schmidt, Dimitris Tsipras, and Adrian Vladu. Towards deep learning models resistant to adversarial attacks. In *International Conference on Learning Representations*, 2018. [2](#), [4](#), [12](#)
- [18] Seyed-Mohsen Moosavi-Dezfooli, Alhussein Fawzi, Omar Fawzi, and Pascal Frossard. Universal adversarial perturbations. In *The IEEE Conference on Computer Vision and Pattern Recognition (CVPR)*, July 2017. [1](#), [7](#)
- [19] Seyed-Mohsen Moosavi-Dezfooli, Alhussein Fawzi, and Pascal Frossard. Deepfool: A simple and accurate method to fool deep neural networks. In *The IEEE Conference on Computer Vision and Pattern Recognition (CVPR)*, June 2016. [1](#), [2](#)
- [20] Muzammal Naseer, Salman H Khan, Harris Khan, Fahad Shahbaz Khan, and Fatih Porikli. Cross-domain transferability of adversarial perturbations. *arXiv preprint arXiv:1905.11736*, 2019. [1](#), [2](#), [5](#), [24](#), [28](#), [29](#)
- [21] Omid Poursaeed, Isay Katsman, Bicheng Gao, and Serge Belongie. Generative adversarial perturbations. In *Proceedings of the IEEE Conference on Computer Vision and Pattern Recognition*, pages 4422–4431, 2018. [1](#), [2](#), [5](#), [28](#)
- [22] Charles R Qi, Wei Liu, Chenxia Wu, Hao Su, and Leonidas J Guibas. Frustum pointnets for 3d object detection from rgb-d data. In *Proceedings of the IEEE Conference on Computer Vision and Pattern Recognition*, pages 918–927, 2018. [1](#)
- [23] Charles R Qi, Hao Su, Kaichun Mo, and Leonidas J Guibas. Pointnet: Deep learning on point sets for 3d classification and segmentation. In *Proceedings of the IEEE Conference on Computer Vision and Pattern Recognition*, pages 652–660, 2017. [1](#), [2](#), [3](#), [5](#), [7](#), [12](#), [16](#), [17](#), [21](#), [24](#), [25](#), [29](#)
- [24] Charles Ruizhongtai Qi, Li Yi, Hao Su, and Leonidas J Guibas. Pointnet++: Deep hierarchical feature learning on point sets in a metric space. In *Advances in neural information processing systems*, pages 5099–5108, 2017. [1](#), [2](#), [3](#), [5](#), [12](#), [16](#), [17](#), [21](#), [22](#)
- [25] Edward Raff, Jared Sylvester, Steven Forsyth, and Mark McLean. Barrage of random transforms for adversarially robust defense. In *The IEEE Conference on Computer Vision and Pattern Recognition (CVPR)*, June 2019. [7](#), [24](#)
- [26] Karen Simonyan and Andrew Zisserman. Very deep convolutional networks for large-scale image recognition. *arXiv preprint arXiv:1409.1556*, 2014. [7](#)
- [27] Christian Szegedy, Wojciech Zaremba, Ilya Sutskever, Joan Bruna, Dumitru Erhan, Ian J. Goodfellow, and Rob Fergus. Intriguing properties of neural networks. *CoRR*, abs/1312.6199, 2013. [1](#), [2](#)
- [28] Maxim Tatarchenko, Jaesik Park, Vladlen Koltun, and Qian-Yi Zhou. Tangent convolutions for dense prediction in 3d. In *Proceedings of the IEEE Conference on Computer Vision and Pattern Recognition*, pages 3887–3896, 2018. [2](#)
- [29] Weiyue Wang, Ronald Yu, Qiangui Huang, and Ulrich Neumann. Sgpn: Similarity group proposal network for 3d point

- cloud instance segmentation. In *Proceedings of the IEEE Conference on Computer Vision and Pattern Recognition*, pages 2569–2578, 2018. 2
- [30] Yue Wang, Yongbin Sun, Ziwei Liu, Sanjay E. Sarma, Michael M. Bronstein, and Justin M. Solomon. Dynamic graph cnn for learning on point clouds. *ACM Transactions on Graphics (TOG)*, 2019. 1, 2, 3, 5, 6, 7, 8, 12, 15, 17, 19, 20, 23, 24, 25, 27
- [31] Zhirong Wu, S. Song, A. Khosla, Fisher Yu, Linguang Zhang, Xiaoou Tang, and J. Xiao. 3d shapenets: A deep representation for volumetric shapes. In *2015 IEEE Conference on Computer Vision and Pattern Recognition (CVPR)*, pages 1912–1920, June 2015. 5, 28
- [32] Chong Xiang, Charles R Qi, and Bo Li. Generating 3d adversarial point clouds. In *Proceedings of the IEEE Conference on Computer Vision and Pattern Recognition*, pages 9136–9144, 2019. 1, 2, 4, 5, 6, 7, 8, 12, 13, 15, 16, 17, 18, 19, 20, 24, 28
- [33] Chaowei Xiao, Dawei Yang, Bo Li, Jia Deng, and Mingyan Liu. Meshadv: Adversarial meshes for visual recognition. In *Proceedings of the IEEE Conference on Computer Vision and Pattern Recognition*, pages 6898–6907, 2019. 2
- [34] Yan Yan, Yuxing Mao, and Bo Li. Second: Sparsely embedded convolutional detection. *Sensors*, 18(10):3337, 2018. 1
- [35] Xiaoqing Ye, Jiamao Li, Hexiao Huang, Liang Du, and Xiaolin Zhang. 3d recurrent neural networks with context fusion for point cloud semantic segmentation. In *European Conference on Computer Vision*, pages 415–430. Springer, 2018. 2
- [36] Lequan Yu, Xianzhi Li, Chi-Wing Fu, Daniel Cohen-Or, and Pheng-Ann Heng. Pu-net: Point cloud upsampling network. In *Proceedings of IEEE Conference on Computer Vision and Pattern Recognition (CVPR)*, 2018. 3
- [37] Xiaohui Zeng, Chenxi Liu, Yu-Siang Wang, Weichao Qiu, Lingxi Xie, Yu-Wing Tai, Chi-Keung Tang, and Alan L. Yuille. Adversarial attacks beyond the image space. In *The IEEE Conference on Computer Vision and Pattern Recognition (CVPR)*, June 2019. 1, 2
- [38] Zhengli Zhao, Dheeru Dua, and Sameer Singh. Generating natural adversarial examples. In *International Conference on Learning Representations*, 2018. 2
- [39] Tianhang Zheng, Changyou Chen, Junsong Yuan, Bo Li, and Kui Ren. Pointcloud saliency maps. In *The IEEE International Conference on Computer Vision (ICCV)*, October 2019. 1, 2, 5
- [40] Hang Zhou, Kejiang Chen, Weiming Zhang, Han Fang, Wenbo Zhou, and Nenghai Yu. Dup-net: Denoiser and upsampler network for 3d adversarial point clouds defense. In *The IEEE International Conference on Computer Vision (ICCV)*, October 2019. 1, 2, 3, 4, 5, 6, 8, 12, 19, 20

A. Background on Point Cloud Distances

We define a point cloud $\mathcal{X} \in \mathbb{R}^{N \times 3}$, as a set of N 3D points, where each point $\mathbf{x}_i \in \mathbb{R}^3$ is represented by its 3D coordinates (x_i, y_i, z_i) . In this work, we focus solely on perturbations of the input. This means we modify each point \mathbf{x}_i by a perturbation variable. Formally, we define the perturbed point set $\mathcal{X}' = \mathcal{X} + \Delta$, where $\Delta \in \mathbb{R}^{N \times 3}$ is the perturbation parameter we are optimizing for. Consequently, each pair $(\mathbf{x}_i, \mathbf{x}'_i)$ are in correspondence.

A.1. Trivial Distances (L_p)

The most commonly used distance metric in adversarial attacks in the image domain. Unlike image domain where every pixel corresponds to the perturbed pixel in adversarial attacks, in point clouds adversarial attacks by adding, removing, or transforming the point cloud destroys the correspondence relation to the clean sample and hence it becomes infeasible to accurately calculate the L_p metric for the attack. In our paper we focus on adversarial perturbations which preserves the matching between the clean sample and the perturbed sample. This property of preservation of matching points allow us to measure the L_p norms of the attack exactly which allow for standard evaluation similar to the one in the image domain. Here we assume the two point sets are equal in size and are aligned, *i.e.* for $\mathbf{x}_i \in \mathcal{X}$, $\mathbf{x}'_i = \mathbf{x}_i + \delta_i$, $i \in 1, 2, \dots, N$

$$\mathcal{D}_{L_p}(\mathcal{X}, \mathcal{X}') = \left(\sum_i \|\delta_i\|_p^p \right)^{\frac{1}{p}} \quad (7)$$

For our attacks, we use the L_2 and L_∞ distances, defined in (8) and (9) respectively. The L_2 distance measures the energy of the perturbation, while L_∞ represents the maximum allowed perturbation of each $\delta_i \in \Delta$.

L_2 distance. The L_2 measures the energy of the perturbation performed on the clean point cloud. Its calculation is similar to calculating the Frobenius norm of the matrix \mathbf{X} that represent the point set perturbation variable Δ such that each row of \mathbf{X} is a point $\delta_i \in \Delta$. The L_2 distance between two point sets can be measured as follows

$$\mathcal{D}_{L_2}(\mathcal{X}, \mathcal{X}') = \left(\sum_i \|\delta_i\|_2^2 \right)^{\frac{1}{2}} = \|\Delta\|_F \quad (8)$$

L_∞ distance. The L_∞ represents the max allowed perturbation at any dimension to every single point δ_i in the perturbation set Δ . This distance between two point sets can be measured as follows :

$$\mathcal{D}_{L_\infty}(\mathcal{X}, \mathcal{X}') = \max_i \|\delta_i\|_\infty \quad (9)$$

A.2. Non-trivial Distances

Other point cloud distances that are commonly used in the literature do not require the two sets to be in a known correspondence (like the strict L_p). These distance metrics include the following: Chamfer Distances, Hausdorff Distance, and Earth Mover Distance. In what follows, we formally present each of these metrics.

Chamfer Distance (CD). This is a common distance to compare 2 point sets. CD measures the average distance between closest point pairs of 2 different point clouds. We define CD in Eq (10).

$$\mathcal{D}_{CD}(\mathcal{X}, \mathcal{X}') = \frac{1}{\|\mathcal{X}'\|_0} \sum_{\mathbf{x}'_i \in \mathcal{X}'} \min_{\mathbf{x}_i \in \mathcal{X}} \|\mathbf{x}_i - \mathbf{x}'_i\|_2 \quad (10)$$

Hausdorff distance (HD). With HD, we compute the largest distance in the set of containing $\mathbf{x} \in \mathcal{X}$ and its closest point $\mathbf{x}' \in \mathcal{X}'$. We define HD as follows:

$$\mathcal{D}_H(\mathcal{X}, \mathcal{X}') = \max_{\mathbf{x}'_i \in \mathcal{X}'} \min_{\mathbf{x}_i \in \mathcal{X}} \|\mathbf{x}_i - \mathbf{x}'_i\|_2 \quad (11)$$

Earth Mover Distance (EMD). The EMD measures the total *effort* performed in the optimal transport scheme that transforms the first point set to the other. It is defined as follows:

$$\mathcal{D}_{EMD}(\mathcal{X}, \mathcal{X}') = \min_{\phi: \mathcal{X} \rightarrow \mathcal{X}'} \sum_i \|\mathbf{x}'_i - \phi(\mathbf{x}_i)\|_2, \quad (12)$$

where $\phi: \mathcal{X} \rightarrow \mathcal{X}'$ is a bijection transform.

B. Our Full Formulation

B.1. Attack Pipeline

Point Cloud Networks (F). We focus on 3D point cloud classifiers with a feature max pooling layer as detailed in Eq (13), where h_{conv1D} and h_{mlp} are a 1D convolution and an MLP, respectively, to produce the K -class classifier \mathbf{F} .

$$\mathbf{F}(\mathcal{X}) = h_{\text{mlp}}(\max_{\mathbf{x}_i \in \mathcal{X}} \{h_{\text{conv1D}}(\mathbf{x}_i)\}) \quad (13)$$

Here $\mathbf{F} : \mathbb{R}^{N \times 3} \rightarrow K$ produces the logits layer of the classifier with size K . For our attacks, we take \mathbf{F} to be one of the following widely used networks in the literature: PointNet [23], PointNet++ [24] in single-scale form (SSG) and multi-scale form (MSG), and DGCNN [30]. Each network manifests different behaviors under random perturbations. Section G.2 delves deep into these differences and their effect on the transferability of the attacks and robustness of each network to perturbations.

Point Cloud Auto-Encoder (G). An AE learns a representation of the data and acts as an effective defense against adversarial attacks. It ideally projects a perturbed point cloud onto the natural manifold of inputs. Any AE architecture in point clouds can be used in our pipeline, but we select the one in [1] given its simple structure and effectiveness in recovering from adversarial perturbation. The AE \mathbf{G} consists of an encoding part, $\mathbf{g}_{\text{encode}} : \mathbb{R}^{N \times 3} \rightarrow \mathbb{R}^q$, which produces a latent vector $\mathbf{z} \in \mathbb{R}^q$ that can in turn be decoded using an MLP, $\mathbf{g}_{\text{mlp}} : \mathbb{R}^q \rightarrow \mathbb{R}^{N \times 3}$, to produce a point cloud. It can be described formally as: $\mathbf{G}(\mathcal{X}) = \mathbf{g}_{\text{mlp}}(\mathbf{z})$ with $\mathbf{z} = \mathbf{g}_{\text{encode}}(\mathcal{X})$. Here, $\mathbf{g}_{\text{encode}}$ is defined as in Eq (13). We train the AE with the Chamfer loss as in [1] on the same data used to train \mathbf{F} , such that it can reliably encode/decode 3D point clouds. The AE is then kept fixed during the optimization of the adversarial perturbation. The AE learns how naturally occurring point clouds look like. Therefore, This composition allows the crafted attack to successfully attack the victim classifier, as well as fool other classifiers that are not seen by the attacker but operate on a similar data manifold. Furthermore, since many of the available points, cloud defenses rely on natural statistics of 3D point clouds [40], succeeding to attack the classifier after AE reconstruction also leads to perturbations resilient to those defenses.

B.2. 3D Adversarial Perturbations

Proposed Attack. Adversarial attacks are commonly formulated as in Eq (14), where the goal is to find an input perturbation Δ that successfully fools \mathbf{F} to predict an incorrect target label t' , while keeping \mathcal{X}' and \mathcal{X} close using distance metric $\mathcal{D} : \mathbb{R}^{N \times 3} \times \mathbb{R}^{N \times 3} \rightarrow \mathbb{R}$. The formulation in Eq (14) is usually known as a targeted attack.

$$\min_{\Delta} \mathcal{D}(\mathcal{X}, \mathcal{X}') \quad \text{s.t.} \quad \left[\max_i \mathbf{F}(\mathcal{X}')_i \right] = t' \quad (14)$$

As pointed out in [3], it is difficult to directly solve Eq (14). Instead, previous works like [32] have used the well-known C&W formulation, giving rise to the commonly known soft constraint attack:

$$\min_{\Delta} f_{t'}(\mathbf{F}(\mathcal{X}')) + \lambda \mathcal{D}(\mathcal{X}, \mathcal{X}') \quad (15)$$

where $\mathcal{D}(\mathcal{X}, \mathcal{X}')$ can be any of the distances proposed in Eq (8,10,12), while $f_{t'}(\mathbf{F}(\mathcal{X}'))$ is the targeted adversarial loss function defined on the network \mathbf{F} to move it to target t' as in Eq (16).

$$f_{t'}(\mathbf{F}(\mathcal{X}')) = \left(\max_{i \neq t'} (\mathbf{F}(\mathcal{X}')_i) - \mathbf{F}(\mathcal{X}')_{t'} \right)^+ \quad (16)$$

Alternatively, we can formulate Eq (14) using hard constraints as in Eq (17), where the objective can be minimized using Projected Gradient Descent (PGD) similar to what is done in the image domain [12, 17].

$$\min_{\Delta} f_{t'}(\mathbf{F}(\mathcal{X}')) \quad \text{s.t.} \quad \mathcal{D}(\mathcal{X}, \mathcal{X}') \leq \epsilon \quad (17)$$

Using a hard constraint sets a limit to the amount of added perturbation in the attack. This limit is defined by ϵ in Eq (17). Having this bound ensures fair comparisons between different attacks schemes. We can do these comparisons by measuring the effectiveness of these attacks at different levels of ϵ . Using PGD, the above optimization in Eq (17) with L_p distance $\mathcal{D}_{L_p}(\mathcal{X}, \mathcal{X}')$ can be solved by iteratively projecting the perturbed sample onto the L_p sphere of size ϵ_p such that:

$$\Delta_{t+1} = \Pi_p(\Delta_t - \eta \nabla_{\Delta_t} f_{t'}(\mathbf{F}(\mathcal{X}')), \epsilon_p) \quad (18)$$

Here, $\Pi_p(\Delta, \epsilon_p)$ projects the perturbation Δ onto the L_p sphere of size ϵ_p , and η is a step size. The two most commonly used L_p distance metrics in the literature are L_2 , which measures the energy of the perturbation, and L_∞ , which measures the maximum point perturbation of each $\delta_i \in \Delta$. Our experiments use the L_2 distance defined as in Eq (8). while the projection of Δ onto the L_2 sphere of size ϵ_2 is:

$$\Pi_2(\Delta, \epsilon_2) = \frac{\epsilon_2}{\max(\|\Delta\|_F, \epsilon_2)} \Delta \quad (19)$$

The norm-budget ϵ_2 is the one used throughout the main paper. On the other hand, the L_∞ projection formulation is as follows:

$$\Pi_\infty(\Delta, \epsilon_\infty) = \text{SAT}_{\epsilon_\infty}(\delta_i), \quad \forall \delta_i \in \Delta, \quad (20)$$

here $\text{SAT}_\zeta(\delta_i)$ is the element-wise saturation function that takes every element of vector δ_i and limit its range in $[-\zeta, \zeta]$.

Data Adversarial Loss. The objectives in Eq (14, 17) focus solely on the network \mathbf{F} . We also want to add more focus

on the data in crafting our attacks. We do so by fooling \mathbf{F} using both the perturbed input \mathcal{X}' and the AE reconstruction $\mathbf{G}(\mathcal{X}')$. Our new objective becomes:

$$\begin{aligned} \min_{\Delta} \mathcal{D}(\mathcal{X}, \mathcal{X}') & \quad (21) \\ \text{s.t. } [\max_i \mathbf{F}(\mathcal{X}')_i] = t'; [\max_i \mathbf{F}(\mathbf{G}(\mathcal{X}'))_i] \neq [\max_i \mathbf{F}(\mathcal{X})_i] \end{aligned}$$

The first constraint is the same as the one in Eq (14), while the second constraint ensures that the prediction of the perturbed sample after the AE differs from the true label of the clean sample. However, just like Eq (14), this objective is hard to optimize, so we follow similar steps as in Eq (17) and optimize for the following main objective of AdvPC using PGD :

$$\begin{aligned} \min_{\Delta} (1 - \gamma) f_{t'}(\mathbf{F}(\mathcal{X}')) + \gamma f_{t''}(\mathbf{F}(\mathbf{G}(\mathcal{X}'))) & \quad (22) \\ \text{s.t. } \mathcal{D}_{L_p}(\mathcal{X}, \mathcal{X}') \leq \epsilon_p \end{aligned}$$

Here, t'' is any false label $t'' \neq \max_i \mathbf{F}(\mathcal{X})_i$ and γ is the hyper-parameter that trades off the attack successes before and after the AE. The baseline attack we use in our experiments is a special case of Eq (22), when $\gamma = 0$. This is the same attack as in Eq (17) and very similar to [32], if put under constraint. We use PGD to solve Eq (22) as follows.

$$\begin{aligned} \Delta_{t+1} = \Pi_p \left(\Delta_t - \eta(1 - \gamma) \nabla_{\Delta_t} f_{t'}(\mathbf{F}(\mathcal{X}')) \right. & \quad (23) \\ \left. - \eta \gamma \nabla_{\Delta_t} f_{t''}(\mathbf{F}(\mathbf{G}(\mathcal{X}'))), \epsilon_p \right) \end{aligned}$$

Where Π_p is the projection to L_p as in Eq (19,20)

We follow the same procedure as in [32] when solving the optimization in Eq (22) by keeping a record of any Δ that satisfies the constraints in Eq (21) and by trying different initializations for Δ . If we achieve the constraints in Eq (21) in one of the optimizations' initializations, we try smaller hard norms in the following initialization in order to find a better solution (smaller norm). This is the exactly the Binary Search followed by [32] to find the best hyperparameter λ in Eq (15) that will result in the smallest norm perturbation that succeeds in the attack on that specific sample. The target t'' is dynamically picked during the optimization to be the max of the logits that is not the true label. This can mean t'' can be equal to the target t' or any other class label that is not the true label $\max_i \mathbf{F}(\mathcal{X})_i$. This is similar to the untargeted attack usually followed in the image domain [12, 6]. The reason we did not pick t'' to be necessarily equal to t' is that it will make the objective in Eq (21) stricter and very hard to optimize and will not converge to a successful attack.

C. Full Qualitative Results

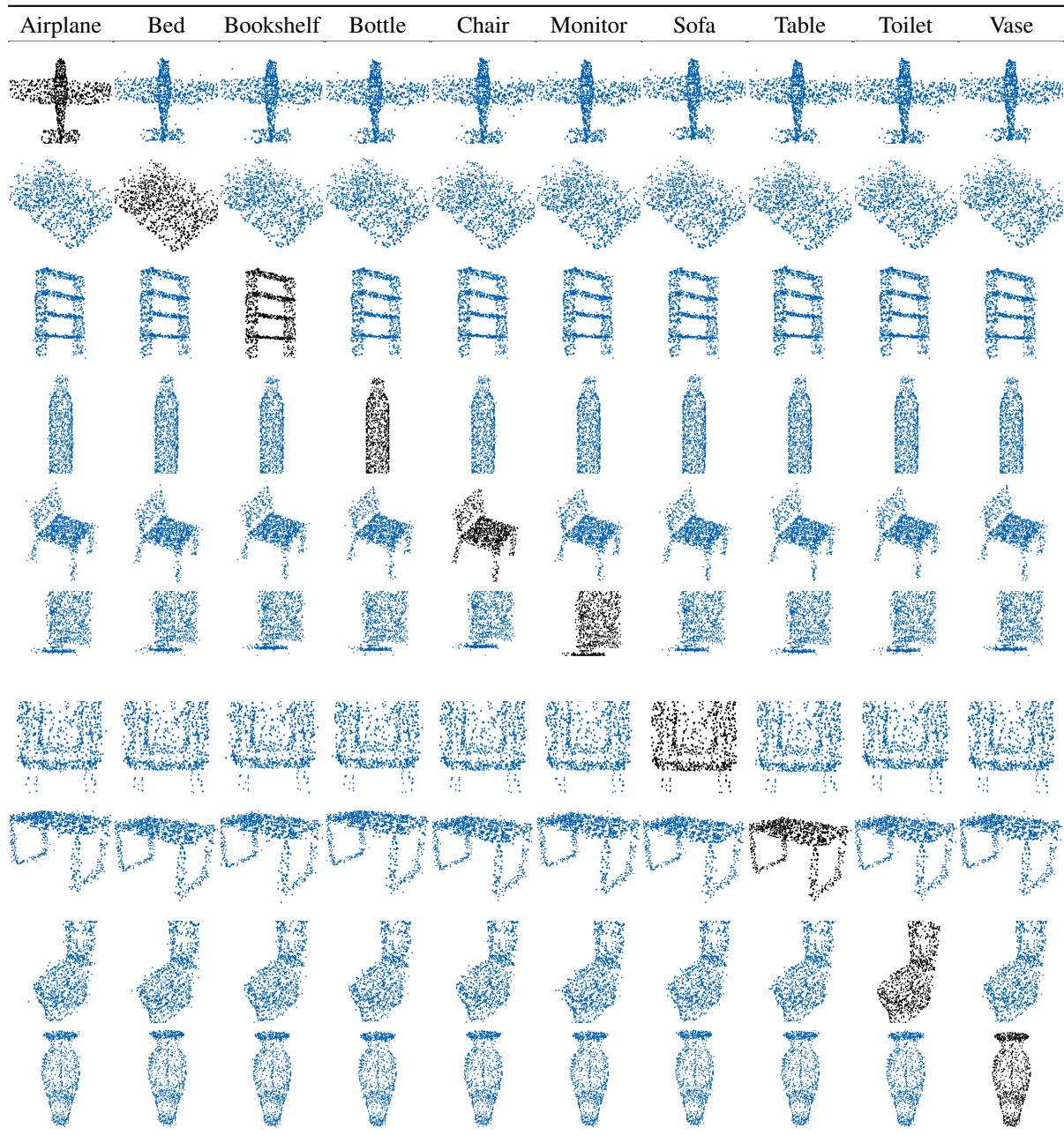


Figure 10: **Examples of AdvPC Attacks:** Adversarial perturbations performed on victim networks PointNet. The original objects are in black under their true class label, while the perturbed examples are in blue under their false target label of the successful attack.

D. Full Transferability Results

D.1. Transferability on Specific Norms

Victim Network	Attack	Success Rate	$\epsilon_2 = 1.8$				$\epsilon_2 = 4$				
			PN	PN++ (MSG)	PN++ (SSG)	DGCNN	Success Rate	PN	PN++ (MSG)	PN++ (SSG)	DGCNN
-	No attack	-	92.8	91.5	91.5	93.7	-	92.8	91.5	91.5	93.7
-	Random	0	73.7	33.3	6.2	46.2	0	32.8	1.7	0.4	0.8
PN	Baseline [32]	100	-	89.7	90.5	93.1	100	-	89.6	90.1	93.1
	AdvPC (Ours)	99.9	-	89.0	86.8	91.0	99.9	-	89.2	88.6	92.5
PN++ (MSG)	Baseline [32]	100	92.4	-	88.1	93.0	100	91.1	-	86.2	92.0
	AdvPC (Ours)	99.2	90.3	-	82.8	91.2	99.2	84.8	-	76.8	83.8
PN++ (SSG)	Baseline [32]	100	92.8	91.7	-	94.4	100	92.8	91.4	-	94.3
	AdvPC (Ours)	100	92.2	91.4	-	94.1	100	92.0	91.1	-	94.4
DGCNN	Baseline [32]	99.6	89.4	88.4	83.0	-	99.7	81.9	87.8	68.8	-
	AdvPC (Ours)	98.3	76.5	77.6	64.6	-	98.3	69.2	70.8	60.0	-

Table 4: **Transferability of Attacks**(L_2): We use norm-budgets $\epsilon_\infty = 1.8$ and $\epsilon_2 = 4$. All the reported results (other than the attack success rate) are classification accuracies on the attack set (**lower** numbers are better attacks). Our attack consistently achieves better transferability than the baseline for all networks, especially on DGCNN [30]. We also note that DGCNN is the hardest network to attack and generally transfers better than other networks. The original accuracy of the networks under no attack, random perturbations with the same ϵ_2 as the attacks, and the success rate of all attacks are all put for reference.

Victim Network	Attack	Success Rate	$\epsilon_\infty = 0.28$				$\epsilon_\infty = 0.35$				
			PN	PN++ (MSG)	PN++ (SSG)	DGCNN	Success Rate	PN	PN++ (MSG)	PN++ (SSG)	DGCNN
-	No attack	-	92.8	91.5	91.5	93.7	-	92.8	91.5	91.5	93.7
-	Random	0	-	-	-	-	0	-	-	-	-
PN	Baseline [32]	100	-	89.2	89.7	92.7	100	-	90.1	89.6	92.5
	AdvPC (Ours)	100	-	86.4	81.8	85.6	100	-	86.8	82.9	87.4
PN++ (MSG)	Baseline [32]	98.0	90.1	-	72.3	86.2	99.1	89.8	-	73.6	86.0
	AdvPC (Ours)	99.2	83.1	-	64.8	78.3	99.5	81.8	-	67.5	78.4
PN++ (SSG)	Baseline [32]	99.8	92.8	91.1	-	94.4	99.9	92.8	91.1	-	94.6
	AdvPC (Ours)	100.0	91.9	91.1	-	93.7	100.0	91.7	90.4	-	94.6
DGCNN	Baseline [32]	94.4	82.0	74.6	60.8	-	96.9	81.9	74.7	60.3	-
	AdvPC (Ours)	90.1	69.2	62.8	48.9	-	91.8	68.6	64.4	50.1	-

Table 5: **Transferability of Attacks**(L_∞): We use norm-budgets $\epsilon_\infty = 0.28$ and $\epsilon_\infty = 0.35$. All the reported results (other than the attack success rate) are classification accuracies on the attack set (**lower** numbers are better attacks). Our attack consistently achieves better transferability than the baseline for all networks, especially on DGCNN [30]. We also note that DGCNN is the hardest network to attack and generally transfers better than other networks. The original accuracy of the networks under no attack, random perturbations with the same ϵ_2 as the attacks, and the success rate of all attacks are all put for reference.

D.2. Different Norms

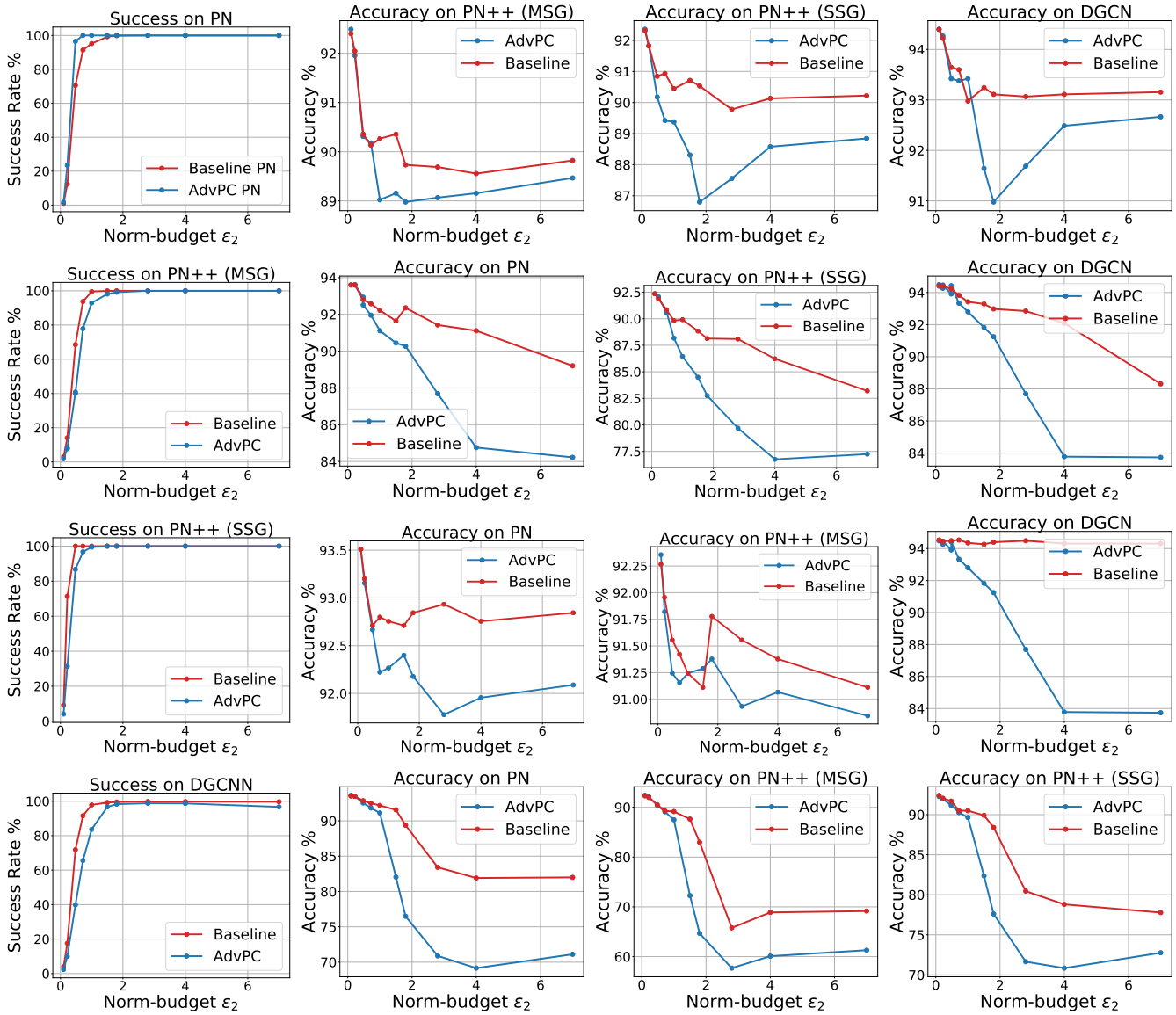


Figure 11: **Transferability Across Different L_2 Norms:** Attack performed using (from top to bottom) PN [23], PointNet ++ MSG, PointNet++ SSG [24] across different ϵ_2 norm-budgets. We report the success on the victim network and the accuracy on the transfer networks (PointNet, PointNet ++ MSG, PointNet++ SSG, DGCNN). We note that AdvPC transfers better to other networks with bigger ϵ_2 compared to the baseline [32].

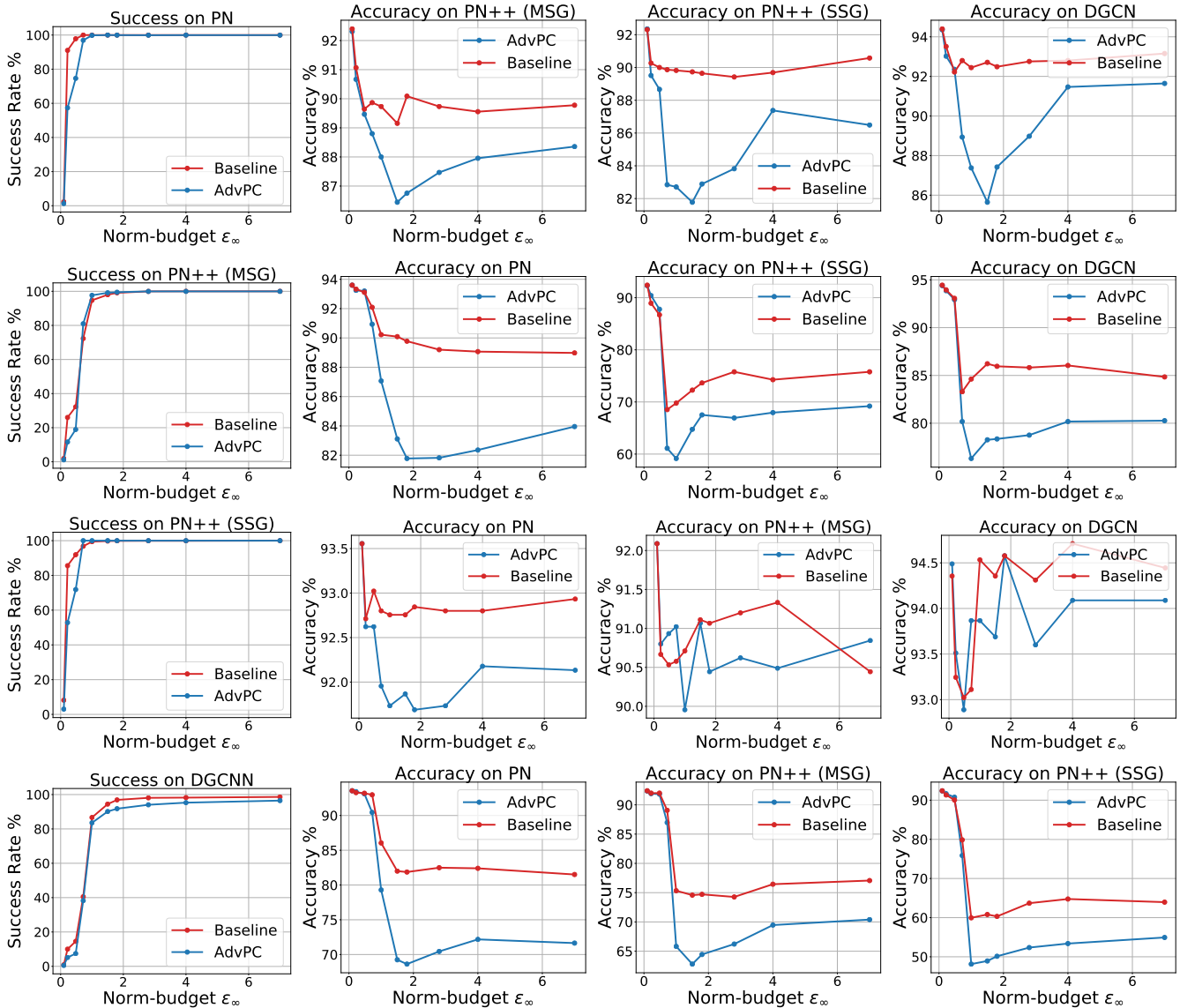


Figure 12: **Transferability Across Different L_∞ Norms:** Attack performed using (from top to bottom) PN [23], PointNet++ MSG, PointNet++ SSG [24] and DGCNN [30] across different ϵ_∞ norm-budgets. We report the success on the victim network and the accuracy on the transfer networks (PointNet, PointNet++ MSG, PointNet++ SSG, DGCNN). We note that AdvPC transfers better to other networks with bigger ϵ_∞ compared to the baseline [32].

D.3. Transferability Matrices

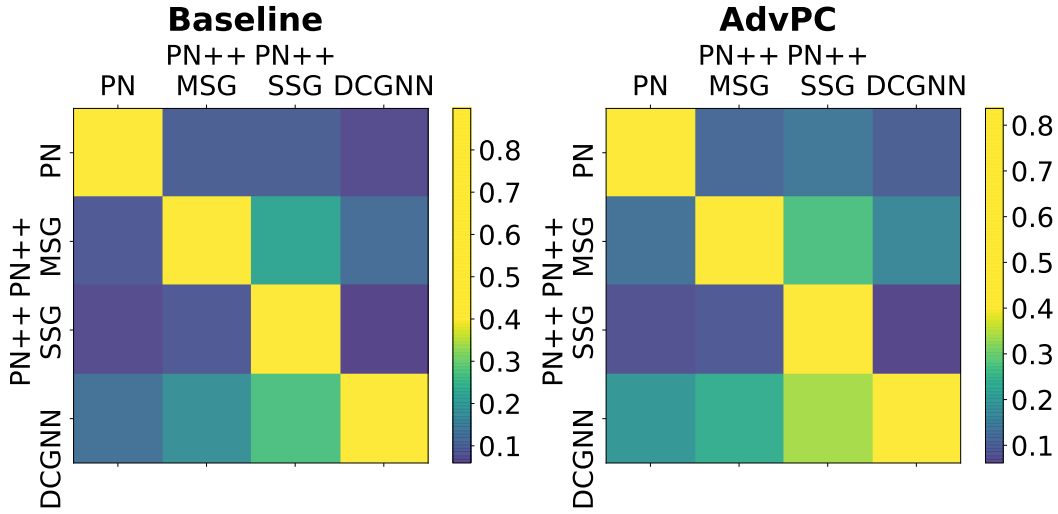


Figure 13: **Transferability Matrix**(L_∞): Visualizing all the transferability across all the norm-budgets ϵ_∞ for AdvPC (right) and Baseline [32] (left). Every row is the victim network used in the attack, and every column is the transfer network transferability score of that attack. Brighter colors in the diagonal indicate self-transferability, while AdvPC transferability matrix is generally brighter than the baseline [32], indicating better transferability. Also, we notice that the DGCNN attacks tend to be brighter off-diagonal than the other rows, indicating more transferability than other networks. The transferability score is 1 minus the average transfer accuracy across all the ϵ_∞ as detailed in Section *Experiments in the main paper*. The transferability of AdvPC: 16.1 % while for the baseline it is 12.6 %.

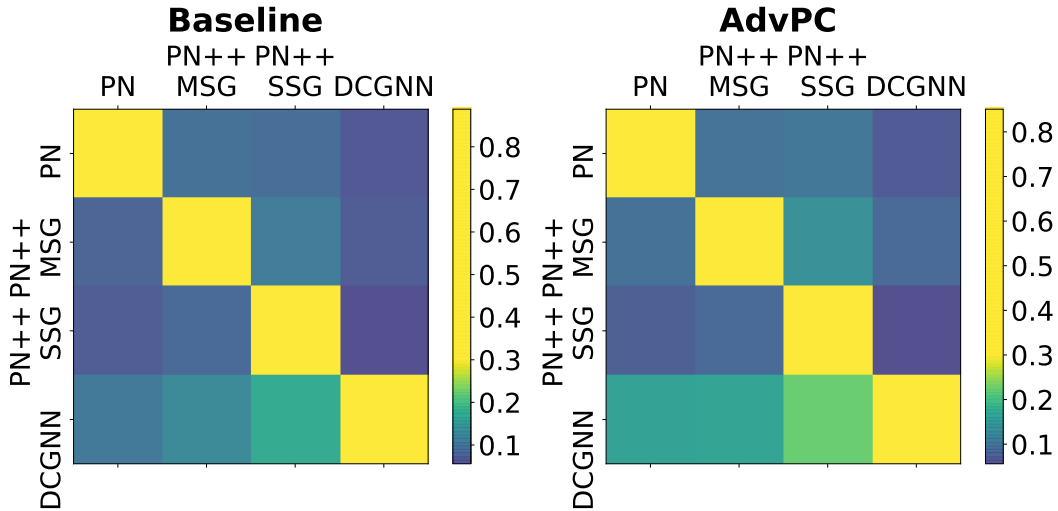


Figure 14: **Transferability Matrix**(L_2): Visualizing all the transferability across all the norm-budgets ϵ_2 for AdvPC (right) and Baseline [32] (left). Every row is the victim network used in the attack, and every column is the transfer network transferability score of that attack. Brighter colors in the diagonal indicate self-transferability, while AdvPC transferability matrix is generally brighter than the baseline [32], indicating better transferability. Also, we notice that the DGCNN attacks tend to be brighter off-diagonal than the other rows, indicating more transferability than other networks. The transferability score is 1 minus the average transfer accuracy across all the ϵ_2 as detailed in Section *Experiments in the main paper*. The transferability of AdvPC: 11.2 % while for the baseline it is 9.4 %.

E. Full Defenses Results

Defenses	$\epsilon_2 = 1.5$		$\epsilon_2 = 1.8$	
	Baseline [32] ($\gamma = 0$)	AdvPC ($\gamma = 0.5$)	Baseline [32] ($\gamma = 0$)	AdvPC ($\gamma = 0.5$)
No defense	0.8	3.3	0.4	1.7
AE	89.5	3.5	88.5	1.7
Adv Training [32]	99.1	97.1	99.0	96.3
SOR [40]	85.7	83.6	84.5	82.0
DUP Net [40]	88.4	87.2	88.0	86.1
SRS [40]	83.2	61.6	75.4	53.2

Table 6: **Attacking Point Cloud Defenses:(DGCNN, L_2)** We evaluate our attack using norm-budgets of $\epsilon_2 = 1.5$ and $\epsilon_2 = 1.8$ using DGCNN [30] on different defenses of 3D point clouds. The reported numbers are accuracies on the attack set (**lower** indicates better attack).

Defenses	$\epsilon_2 = 1.5$		$\epsilon_2 = 1.8$	
	Baseline [32] ($\gamma = 0$)	AdvPC ($\gamma = 0.5$)	Baseline [32] ($\gamma = 0$)	AdvPC ($\gamma = 0.5$)
No defense	0.0	0.7	0.0	0.1
AE	90.9	0.8	90.7	0.1
Adv Training [32]	91.6	90.8	91.2	90.4
SOR [40]	87.8	89.9	88.6	90.7
DUP Net [40]	91.2	91.2	91.0	91.1
SRS [40]	69.0	60.9	63.6	59.4

Table 7: **Attacking Point Cloud Defenses:(PointNet, L_2)** We evaluate our attack using norm-budgets of $\epsilon_2 = 1.5$ and $\epsilon_2 = 1.8$ using DGCNN [30] on different defenses of 3D point clouds. The reported numbers are accuracies on the attack set (**lower** indicates better attack).

Defenses	$\epsilon_2 = 1.5$		$\epsilon_2 = 1.8$	
	Baseline [32] ($\gamma = 0$)	AdvPC ($\gamma = 0.5$)	Baseline [32] ($\gamma = 0$)	AdvPC ($\gamma = 0.5$)
No defense	0.0	1.8	0.0	0.8
AE	88.8	1.9	88.7	0.8
Adv Training [32]	99.3	98.7	98.5	98.5
SOR [40]	85.9	84.8	84.3	85.1
DUP Net [40]	86.0	86.0	86.3	86.4
SRS [40]	82.2	80.3	79.9	78.0

Table 8: **Attacking Point Cloud Defenses:(PointNet++MSG, L_2)** We evaluate our attack using norm-budgets of $\epsilon_2 = 1.5$ and $\epsilon_2 = 1.8$ using DGCNN [30] on different defenses of 3D point clouds. The reported numbers are accuracies on the attack set (**lower** indicates better attack).

Defenses	$\epsilon_2 = 1.5$		$\epsilon_2 = 1.8$	
	Baseline [32] ($\gamma = 0$)	AdvPC ($\gamma = 0.5$)	Baseline [32] ($\gamma = 0$)	AdvPC ($\gamma = 0.5$)
No defense	0.0	0.0	0.0	0.0
AE	83.0	9.1	81.9	7.4
Adv Training [32]	94.1	92.3	93.4	92.4
SOR [40]	76.0	77.6	75.6	79.0
DUP Net [40]	88.4	88.3	87.8	87.3
SRS [40]	56.3	47.2	58.1	48.6

Table 9: **Attacking Point Cloud Defenses:(PointNet++SSG, L_2)** We evaluate our attack using norm-budgets of $\epsilon_2 = 1.5$ and $\epsilon_2 = 1.8$ using DGCNN [30] on different defenses of 3D point clouds. The reported numbers are accuracies on the attack set (**lower** indicates better attack).

Defenses	$\epsilon_\infty = 0.18$		$\epsilon_\infty = 0.28$	
	Baseline [32] ($\gamma = 0$)	AdvPC ($\gamma = 0.5$)	Baseline [32] ($\gamma = 0$)	AdvPC ($\gamma = 0.5$)
No defense	12.6	15.7	5.3	9.4
AE	87.1	0.0	87.6	0.0
Adv Training [32]	99.2	98.1	99.2	97.5
SOR [40]	85.4	85.2	85.3	85.4
DUP Net [40]	80.1	80.5	81.2	81.3
SRS [40]	85.7	75.7	84.0	76.3

Table 10: **Attacking Point Cloud Defenses:(DGCN, L_∞)** We evaluate our attack using norm-budgets of $\epsilon_\infty = 0.18$ and $\epsilon_\infty = 0.28$ using DGCNN [30] on different defenses of 3D point clouds. The reported numbers are accuracies on the attack set (**lower** indicates better attack).

Defenses	$\epsilon_\infty = 0.18$		$\epsilon_\infty = 0.28$	
	Baseline [32] ($\gamma = 0$)	AdvPC ($\gamma = 0.5$)	Baseline [32] ($\gamma = 0$)	AdvPC ($\gamma = 0.5$)
No defense	0	0.1	0	0
AE	90.4	0.0	90.9	0.0
Adv Training [32]	90.5	87.5	90.5	88.2
SOR [40]	90.4	90.6	90.8	91.2
DUP Net [40]	91.0	91.2	91.4	91.0
SRS [40]	57.9	49.2	58.6	50.0

Table 11: **Attacking Point Cloud Defenses:(PointNet, L_∞)** We evaluate our attack using norm-budgets of $\epsilon_\infty = 0.18$ and $\epsilon_\infty = 0.28$ using DGCNN [30] on different defenses of 3D point clouds. The reported numbers are accuracies on the attack set (**lower** indicates better attack).

Defenses	$\epsilon_\infty = 0.18$		$\epsilon_\infty = 0.28$	
	Baseline [32] ($\gamma = 0$)	AdvPC ($\gamma = 0.5$)	Baseline [32] ($\gamma = 0$)	AdvPC ($\gamma = 0.5$)
No defense	4.88	2.26	1.95	0.8
AE	87.2	0.7	86.8	0.4
Adv Training [32]	97.2	95.8	96.9	96.4
SOR [40]	73.2	82.3	75.5	82.4
DUP Net [40]	79.8	83.7	81.5	81.5
SRS [40]	69.5	61.0	69.6	61.1

Table 12: **Attacking Point Cloud Defenses:(PointNet++MSG, L_∞)** We evaluate our attack using norm-budgets of $\epsilon_\infty = 0.18$ and $\epsilon_\infty = 0.28$ using DGCNN [30] on different defenses of 3D point clouds. The reported numbers are accuracies on the attack set (**lower** indicates better attack).

Defenses	$\epsilon_\infty = 0.18$		$\epsilon_\infty = 0.28$	
	Baseline [32] ($\gamma = 0$)	AdvPC ($\gamma = 0.5$)	Baseline [32] ($\gamma = 0$)	AdvPC ($\gamma = 0.5$)
No defense	0.5	0.0	0.2	0.0
AE	86.1	0.0	87.4	0.0
Adv Training [32]	97.6	96.7	97.8	96.8
SOR [40]	85.4	86.9	85.7	86.9
DUP Net [40]	86.7	87.1	88.1	88.9
SRS [40]	74.0	67.7	71.2	69.1

Table 13: **Attacking Point Cloud Defenses:(PointNet++ SSG, L_∞)** We evaluate our attack using norm-budgets of $\epsilon_\infty = 0.18$ and $\epsilon_\infty = 0.28$ using DGCNN [30] on different defenses of 3D point clouds. The reported numbers are accuracies on the attack set (**lower** indicates better attack).

F. Ablation Study on the Losses

We ablate each component of our pipeline and show their effect in our attacks. We evaluate this components by looking Attack Success Rate (ASR), transferability, and the final norm obtained under the attack. In these experiments, we fix the attack network to be PointNet++ MSG and allow unconstrained attacks as well as constrained attacks. We show the effect of optimizing using EMD, CD, L_2 , and L_∞ . We show the results on Tables 14,15,16,17 for all the four networks. We observe transferability is better when using hard constraints. Constraining the attack norm allows the optimization to learn more from the AE data distribution. The EMD doesn't work well while the Chamfer loss is comparable to the L_2 loss.

soft CD	soft EMD	Attack Setup				AE	Results					
		soft L_2	hard L_∞	hard L_2			CD	EMD	L_∞	L_2	ASR	Transferability
✓	-	-	-	-	-	0.15	4.25	0.12	0.31	100.00	9.02	
✓	-	-	-	-	✓	0.19	5.01	0.13	0.36	99.69	9.51	
-	✓	-	-	-	-	0.17	2.83	0.23	0.39	68.36	9.01	
-	✓	-	-	-	✓	0.16	2.53	0.25	0.37	18.04	7.35	
-	-	✓	-	-	-	0.16	4.38	0.11	0.31	100.00	8.92	
-	-	✓	-	-	✓	0.21	5.22	0.13	0.36	100.00	9.35	
-	-	-	✓	-	-	0.49	12.37	0.04	0.55	100.00	9.16	
-	-	-	✓	-	✓	0.73	13.66	0.07	0.72	96.93	13.14	
-	-	-	-	✓	-	0.26	7.41	0.09	0.38	100.00	8.87	
-	-	-	-	✓	✓	0.37	7.35	0.16	0.48	99.87	11.08	

Table 14: **Soft vs Hard on PointNet**: study the effect of every bit of the loss on the norms and success rate under unconstrained setup vs constrained setup in PointNet [23].($\epsilon_\infty = 0.1$, $\epsilon_2 = 1.8$), $\lambda = 1, \gamma = 0.5$. Please refer to Section B for details. **Bold** numbers are the best.

soft CD	soft EMD	Attack Setup				AE	Results					
		soft L_2	hard L_∞	hard L_2			CD	EMD	L_∞	L_2	ASR	Transferability
✓	-	-	-	-	-	1.01	25.80	0.19	1.00	99.78	11.57	
✓	-	-	-	-	✓	0.88	26.25	0.21	1.15	95.69	12.19	
-	✓	-	-	-	-	0.21	5.04	0.23	0.56	14.58	6.83	
-	✓	-	-	-	✓	0.07	2.23	0.12	0.20	2.31	6.61	
-	-	✓	-	-	-	1.35	26.58	0.20	0.96	99.96	13.38	
-	-	✓	-	-	✓	1.43	26.42	0.22	0.98	100.00	16.61	
-	-	-	✓	-	-	3.71	53.83	0.06	1.84	94.71	18.46	
-	-	-	✓	-	✓	2.53	38.78	0.10	1.45	97.64	25.82	
-	-	-	-	✓	-	0.59	15.95	0.10	0.58	100.00	8.84	
-	-	-	-	✓	✓	0.93	20.08	0.15	0.75	99.20	11.91	

Table 15: **Soft vs Hard on PointNet++ MSG**: study the effect of every bit of the loss on the norms and success rate under unconstrained setup vs constrained setup in PointNet++ MSG [24]. ($\epsilon_\infty = 0.18$, $\epsilon_2 = 1.8$), $\lambda = 1, \gamma = 0.5$. Please refer to Section B for details. **Bold** numbers are the best.

Attack Setup						Results					
soft CD	soft EMD	soft L_2	hard L_∞	hard L_2	AE	CD	EMD	L_∞	L_2	ASR	Transferability
✓	-	-	-	-	-	0.25	9.39	0.07	0.37	100.00	7.01
✓	-	-	-	-	✓	0.25	9.38	0.08	0.39	99.51	7.17
-	✓	-	-	-	-	0.08	3.71	0.09	0.28	37.20	6.74
-	✓	-	-	-	✓	0.07	2.95	0.10	0.24	4.84	6.52
-	-	✓	-	-	-	0.30	9.90	0.07	0.39	100.00	6.92
-	-	✓	-	-	✓	0.28	9.63	0.07	0.38	100.00	7.56
-	-	-	✓	-	-	1.20	24.52	0.02	0.83	96.80	7.84
-	-	-	✓	-	✓	0.80	17.24	0.05	0.70	100.00	7.72
-	-	-	-	✓	-	0.19	8.08	0.04	0.30	100.00	6.99
-	-	-	-	✓	✓	0.46	12.42	0.09	0.50	100.00	7.44

Table 16: **Soft vs Hard on PointNet++ SSG**: study the effect of every bit of the loss on the norms and success rate under unconstrained setup vs constrained setup in PointNet++ SSG [24].($\epsilon_\infty = 0.1$, $\epsilon_2 = 1.8$), $\lambda = 1, \gamma = 0.5$. Please refer to Section B for details. **Bold** numbers are the best.

soft CD	soft EMD	Attack Setup				AE	Results					
		soft L_2	hard L_∞	hard L_2			CD	EMD	L_∞	L_2	ASR	Transferability
✓	-	-	-	-	-	1.06	32.22	0.20	1.55	67.91	10.46	
✓	-	-	-	-	✓	0.71	25.03	0.17	1.18	41.07	9.21	
-	✓	-	-	-	-	0.03	2.47	0.07	0.14	2.07	7.18	
-	✓	-	-	-	✓	0.01	1.62	0.01	0.05	0.76	7.21	
-	-	✓	-	-	-	2.81	39.95	0.28	1.53	99.20	23.23	
-	-	✓	-	-	✓	2.89	40.55	0.31	1.58	96.89	29.91	
-	-	-	✓	-	-	4.39	53.49	0.12	2.12	86.67	26.22	
-	-	-	✓	-	✓	5.10	58.24	0.16	2.40	83.56	35.59	
-	-	-	-	✓	-	2.46	39.85	0.23	1.45	99.82	23.45	
-	-	-	-	✓	✓	2.82	43.19	0.30	1.63	98.80	33.26	

Table 17: **Soft vs Hard on DGCNN**: study the effect of every bit of the loss on the norms and success rate under unconstrained setup vs constrained setup in DGCNN [30]. ($\epsilon_\infty = 0.18$, $\epsilon_2 = 2.8$), $\lambda = 1, \gamma = 0.5$. Please refer to Section B for details. **Bold** numbers are the best.

G. Analysis of the results

The transferability of attacks lies in the difficulty domain of attacks as Figure 15 illustrates. We perform several analytical experiments to explore further the results obtained in so far. We first study the effect of different factors that play a role in the transferability of our attacks. We also show some interesting insights related to the interpretability of point cloud networks.

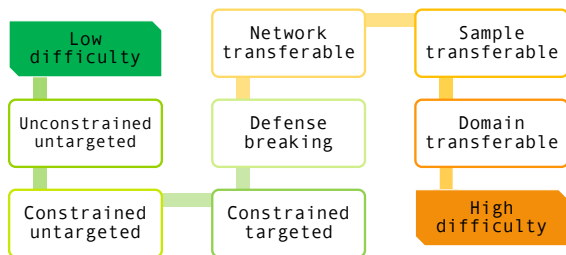


Figure 15: **Difficulty of Adversarial Attacks:** Attacking trained networks differ in difficulty according to the setup used in the attack. Allowing bigger perturbations for the attack or not specifying a target make it easier, while requiring transferability of the attack to different networks is a challenging in the study of robustness [20]

G.1. Ablation Study of Hyperparameter γ

Here, we study the effect of the hyperparameter γ used in Eq (22) on the performance of our attacks. We fix the victim network to be DGCNN [30] and limit the norm-budget $\epsilon_2 = 1.8$. Then, we vary γ between 0 (the baseline [32]) and 1 and record the success rate and transferability of the attack to the other three networks. The transferability is measured here for each network as 1 minus the average transfer accuracy of the attack to the other three networks. We present our results in Figure 16. One observation is that, while adding the AE loss with $\gamma > 0$ indeed improves transferability, it causes the success to deteriorate. We pick $\gamma = 0.5$ in our experiments to balance success and transferability. The trend in general is that bigger γ implies better transferability with loss in the success rate

G.2. Sensitivity of Networks

Figure 17 shows the sensitivity of the various networks, when they are submitted to input perturbations of varying norm-budgets ϵ_2 . We evaluate the accuracy of different networks under random perturbation and adversarial perturbations with $\gamma = 0.5$. We note that PointNet [23] is the most robust under random perturbations due to its global max-pooling layer that neglects neighborhood information of each point in the point cloud. On the other hand, DGCNN [30] tends to be the most robust to adversarial perturbations.

Original	Closest class	Original	Closest class
Airplane	Plant	Monitor	Bed
Bed	Sofa	Sofa	Bed
Bookshelf	Curtain	Table	Bed
Bottle	Vase	Toilet	Plant
Chair	Plant	Vase	Bottle

Table 18: **Semantic Links:** Association between object before and after reconstruction with the AE. We record most repeated prediction after reconstruction of AdvPC attacked samples with $\epsilon_2 = 1.8$ on DGCNN [30]. This shows subjective links between object classes that are similar to humans judgement in linking different classes.

In DGCNN, convolution neighborhoods are dynamically updated across layers and epochs. This dynamic behavior adds extra randomness, which hinders the job of the attack, leading to lower success. The relation between randomness and robustness is also established in [25]. Figure 18 shows similar results under L_∞ norms instead of the L_2 norm-budgets. We observe similar pattern between Figure 17 and Figure 18.

G.3. Interpretability

One advantage of adding the AE to the attack pipeline is that it reveals some semantic relations between the different object classes. Since we are not enforcing a specific false target t'' for the data adversarial loss on the reconstructed point cloud in Eq (22), t'' is picked dynamically by the optimization to be a *similar* class to the original class. For example, a perturbed Bottle by AdvPC would transform into a Vase if reconstructed by the AE. The Bottle class and the Vase class looks *similar*. We see this effect in Figure 19, where we visualize the perturbed point clouds before and after the AE reconstruction. For example, we observe that our attacks on a *bottle* force the AE to reconstruct a *vase*. This effect is not observed in the other attacks, and it illustrates some information about the representation of the objects learned by the victim network as well as the AE. In Table 18, we show the closest class pairs for different object classes from ModelNet40 observed in AdvPC attacks.

G.4. Accuracy vs. Robustness

In order to factor out the effect of the initial accuracy of the network on the study of robustness, we divide the accuracy under perturbation by the initial accuracy of the network. If we use DGCN [30] as our main network and train it for different epochs, we obtain identical networks that have different initial accuracies (on clean samples). Now we plot the normalized test accuracy under random perturbation with different ϵ_∞ for all the networks (Figure 20). We observe how less accurate networks are more resilient to attacks. This inverse relation between accuracy and robustness is well known in the image domain.

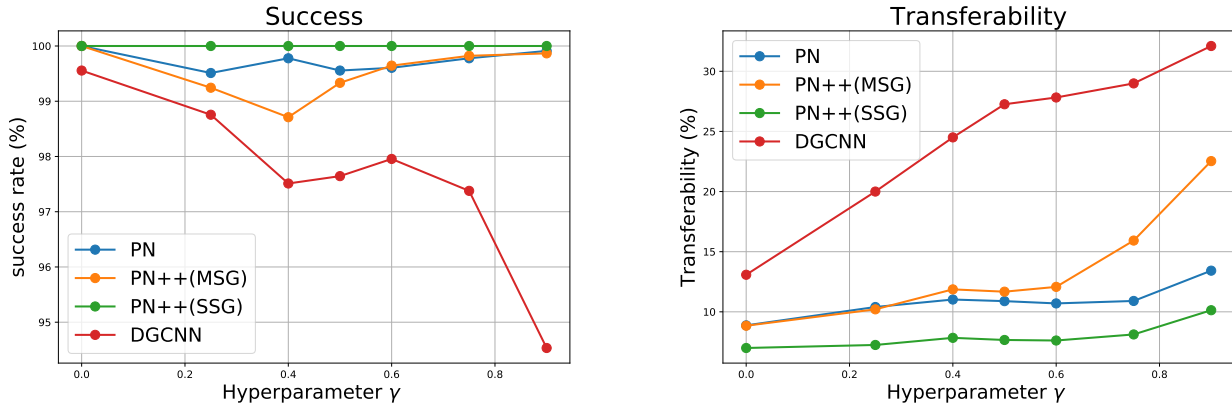


Figure 16: **Ablation Study:** Studying the effect of changing the hyperparameter in our attack (γ) on the success rate of the attack and on its transferability (1- average accuracy of transfer networks). The attacks performed with $\epsilon_2 = 1.8$. We note that as γ increases, the success rate of the attack drops while the transferability increases, which highlights the trade-off between success and transferability observed throughout our work.

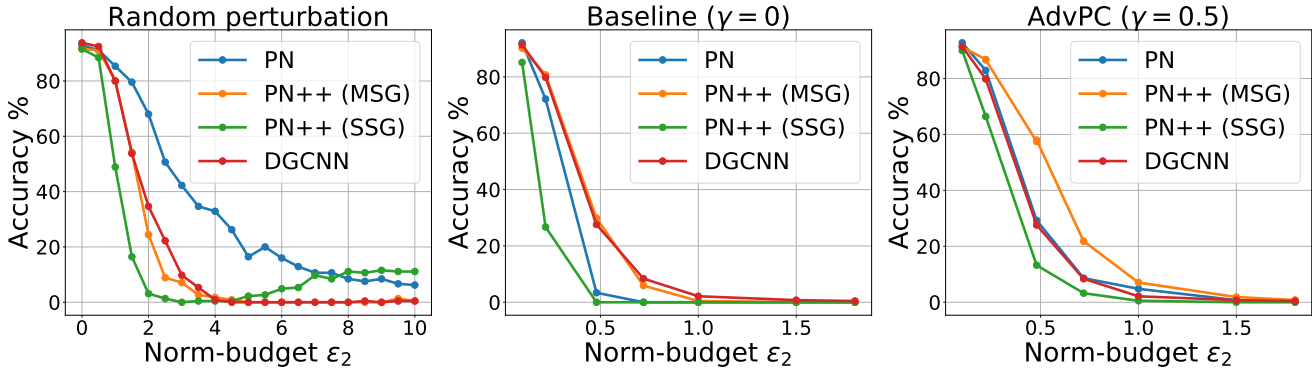


Figure 17: **Sensitivity of Architectures:** we evaluate the accuracy of different networks under constrained norm random perturbation (*left*), adversarial perturbation (*middle*) with $\gamma = 0.0$ and adversarial perturbation (*right*) with $\gamma = 0.5$ across all the norm-budgets L_2 . We note that PointNet [23] is the most robust under random perturbations, while DGCNN [30] is the most robust to adversarial perturbations.

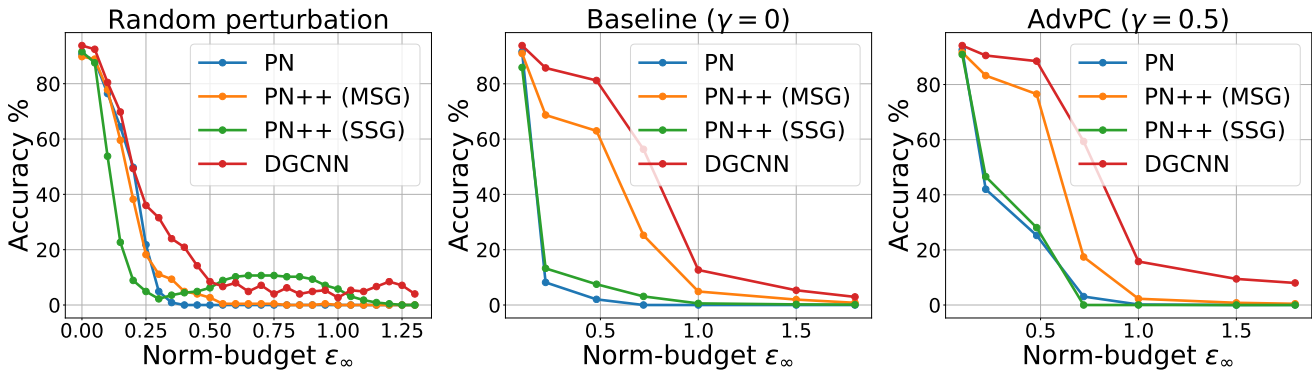


Figure 18: **Sensitivity of Architectures:** we evaluate the accuracy of different networks under constrained norm random perturbation (*left*), adversarial perturbation (*middle*) with $\gamma = 0.0$ and adversarial perturbation (*right*) with $\gamma = 0.5$ across all the norm-budgets L_∞ . We note that DGCNN [30] is the most robust to random and adversarial perturbations.

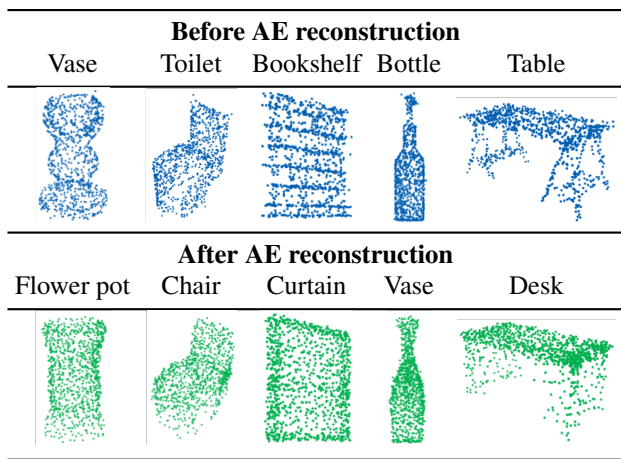


Figure 19: **Interpretability of AdvPC:** Attacked samples before reconstruction (*top*) and after reconstruction (*bottom*) by the AE. Perturbed samples by AdvPC, if passed through the AE, transform into similar objects but from different classes. This illustrates some information about what the representation learned by the victim network and the AE.

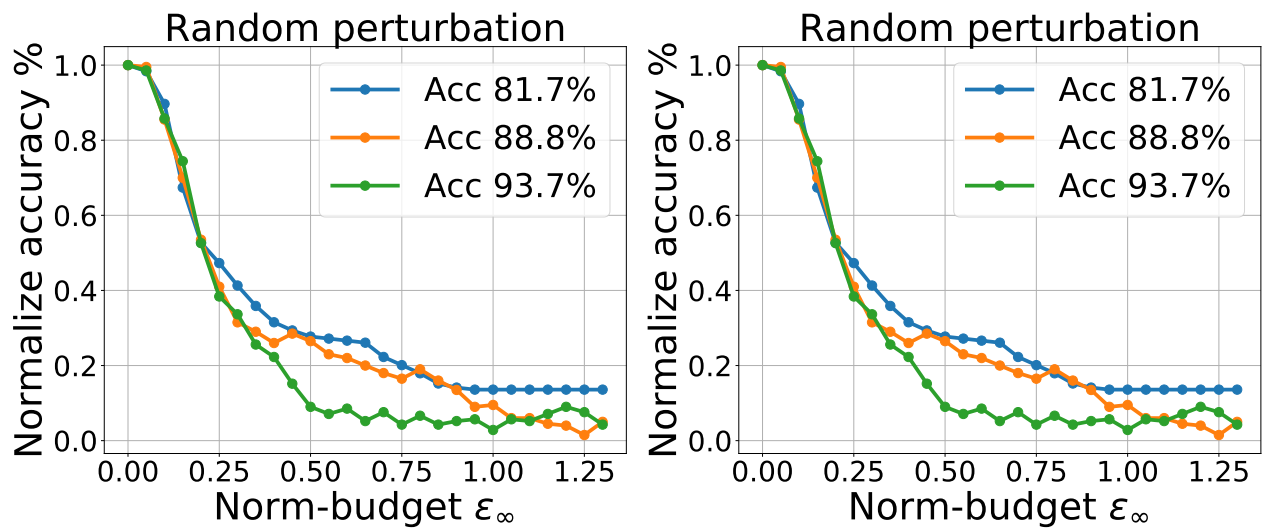


Figure 20: **Accuracy vs Robustness:** The normalized accuracy of different DGCNN [30] trained with different accuracies and evaluated under random perturbations (*left*) and adversarial perturbation with $\gamma = 0.5$ (*right*) across all the norm-budgets L_∞ .

H. Other Tried Approaches (Less Successful)

H.1. Point Cloud GAN:

We try to use the l-GAN and r-GAN from [1] in order to create more natural attacks to the input point clouds. We try to leverage the discriminator signal of both r-GAN and l-GAN in order to differentiate between the perturbed point clouds and the original samples. The idea is that if the trained discriminator is able to distinguish between the clean and attacked sample than we add the discriminator loss as an additional loss to the attack objective in Eq (17) in order to craft that pass the trained discriminator test of natural input. We train l-GAN and r-GAN with the same procedure advised by [1] and on the same data as our AE \mathcal{G} . However, as Figure 21 illustrates, neither l-GAN nor r-GAN were able to distinguish between the clean samples and the perturbed samples using the attack from [32]. This disappointing result lead us to abandon the approach in favour of the AE optimization (which works).

H.2. Learning Approach

Inspired by the success of [20, 21] in learning to attack, we tried to learn the AE \mathcal{G} that will produce the desired perturbed point cloud \mathcal{X}' by optimizing the output of the AE by the soft adversarial loss. To achieve this, the AE should output points clouds that are close as possible to the input point cloud \mathcal{X} (by the Chamfer soft loss as in Eq (15)) and also the output of the AE should fool the classifier \mathbf{F} . We note that because of the nature of point cloud, we could not project the output of the AE back to the original sample with some norm, as performed by [20], and hence we used the soft Chamfer loss instead. We train the AE to perform untargeted and targeted attacks on the training set of ModelNet40 [31] and evaluate the adversary \mathcal{G} on the test set of ModelNet. We report the results of targeted and untargeted attacks in Table 19. We note that while the untargeted attacks did succeed in deteriorating the accuracy to almost 10 % , the targeted attack never really succeeding in attacks (compared to our results in Table 4,5). Also, even for the untargeted attacks that indeed succeed, the final Chamfer Distance is way bigger than the ones obtained by optimization (see Tables 14). This might be attributed to the difficulty of learning an attack that works under varying distance penalties, unlike the [20] where the adversarial objective is hardly conditioned on a constant distance between the attacked image and the original image.

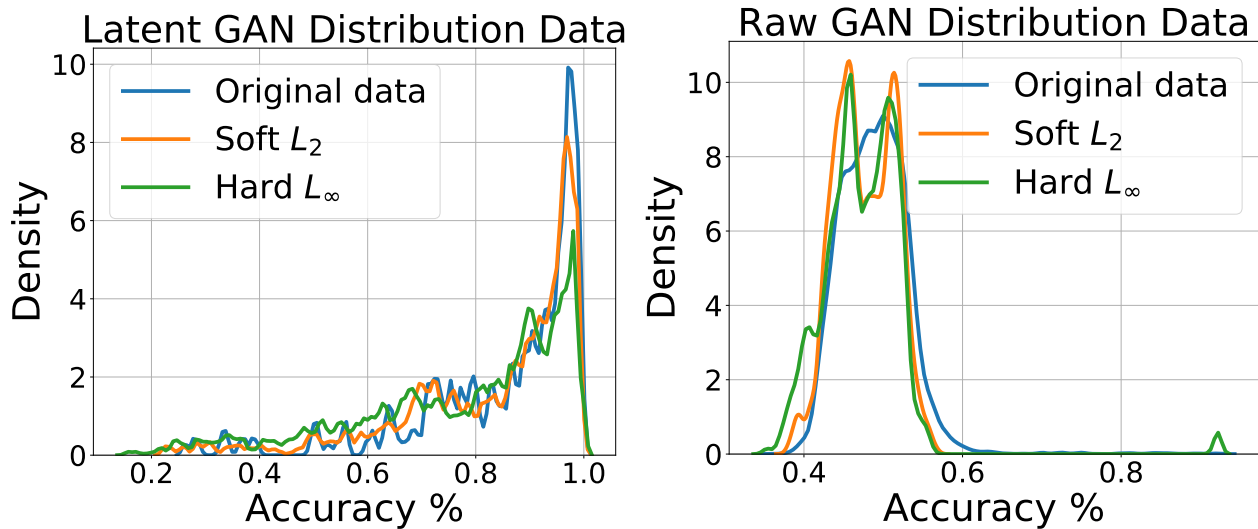


Figure 21: **GAN instead of AE:** We tried to use l-GAN and r-GAN from [1] as natural priors for AdvPC attacks instead of the AE. The discriminators of Both l-GAN and r-GAN could not discriminate between the original data and the attacks data by soft L_2 loss or Hard L_∞ . We show the histogram distribution of discriminator scores of the original data and attacked data using l-GAN discriminator (*left*) and r-GAN discriminator (*right*).

Loss	soft hyperparameter λ_{CD}	Learning rate	Untargeted/Targeted	Training Epochs	Accuracy	Chamfer Distance
Relativistic	0	0.0001	Untargeted	15	6.375	2.6161
Relativistic	1	0.0001	Untargeted	15	5.0833	2.4832
Relativistic	3	0.0001	Untargeted	13	9.9167	0.024229
Relativistic	10	0.0001	Untargeted	13	8.9583	0.022948
Relativistic	30	0.0001	Untargeted	13	10.125	0.021558
Relativistic	100	0.0001	Untargeted	13	13.625	0.018275
Relativistic	300	0.0001	Untargeted	16	17.875	0.014084
Relativistic	1000	0.0001	Untargeted	13	38.0417	0.09286
Relativistic	0	0.00005	Untargeted	13	9.7083	0.023431
Relativistic	0	0.0001	Targeted	0	81.5	0.005556
Relativistic	0	0.001	Targeted	19	31.875	0.015868

Table 19: **The Learning Approach on PointNet:** We tried to learn a network to attack PointNet [23] (approach similar to [20] but on point clouds). While the approach mildly succeeds on untargeted attacks, the final average Chamfer distance on the succeeding attacks are much bigger than those obtained by optimization like in Figure 14. This implies that the optimization is actually better on point clouds.